CHAPTER 1. INTRODUCTION

1.1. General

The sun is the greatest source of energy. The small fraction of solar irradiation received by the earth is sufficient for the existence of life. This irradiation is converted into different forms of energy that are useful in many different applications. All the other sources of energy known to exist have their origin as the sun except for nuclear energy. The advantages of the sun have led many scientists throughout the world to research on economic ways of harnessing its energy.

The sun is a renewable source of energy. It is relatively easy to harness and is environmentally friendly. These advantages make it a number one candidate for the provision of energy to the whole world. Coal and oil have been used for many years now and have proved to be detrimental to our environment. The burning of these fossil fuels leads to emission of carbon dioxide, sulphur and nitrous oxides. Carbon dioxide is a strong greenhouse gas that causes global warming. Sulphur and nitrous oxides are converted into acids in the atmosphere and are eventually precipitated as acid rain, which is dangerous to animals and plants. Nuclear energy is not environmentally friendly and has drawbacks since the nuclear power plants are expensive to built and maintain. Furthermore, the storage and disposal of nuclear waster has not been resolved yet.

Many solar collecting devices are already in use throughout the world. These collect solar radiation and convert it into useful energy such as heat or electricity. Photo-voltaic devices use semiconducting materials to convert sunlight directly into electricity. Photo-thermal devices usually called solar collectors convert solar radiation into heat (thermal conversion). Solar

collectors are used to heat water and air inside buildings at lower temperatures (T<300 °C) and to create steam for electricity generation at high temperatures (T>300 °C).

Solar collectors used for heating water and air conditioning are mainly of flat-plate type [1,2]. A flat-plate solar collectors is simple and inexpensive. The most important and critical part of the flat plate collectors is the absorber surface. In order to maximize the output from the solar collectors, the absorber should be spectrally selective. It should absorb as much of the incoming solar radiation as possible and at the same time retain the collected heat. This means that it should exhibit high solar absorptance and low thermal emittance. Thermal losses due to conduction, convection and radiation have an effect on the efficiency of solar absorbers. Other desirable properties of solar absorbers are that they should not degrade significantly during the lifetime of the collector and that they should withstand harsh environmental conditions.

One of the approaches being used to reduce the cost of solar absorbing systems is to increase the working temperature from approximately 400 °C to 500 °C or higher [3]. New types of efficient spectrally selective coatings that have both high solar absorptance and low thermal emittance at 500 °C are needed to accomplish this. Currently solar absorber coatings do not have the stability and performance desired for moving to higher operating temperatures. The condition for high solar absorbance and low thermal emittance at the operational temperature of these absorbers is of much concern in the efficient photo-thermal conversion.

There exist many types of selective solar absorbers. The most common type of selective absorber is the absorber-reflector tandem which is obtained by combining two surfaces, one surface which is highly absorbing in the solar region and another highly reflecting in the infrared region so that

the thermal losses can be minimised. Some metal substrates such as aluminium, copper and stainless steel are used in the absorber because of their high thermal conductivity. These metals have a high infrared reflectance, which makes them suitable as the infrared reflector in the tandem absorber. Their disadvantage is that they are sensitive to corrosion and if the absorbing layer does not function as a protecting layer, a specific layer has to be added. Gelin [4] did a research on the optimisation and improvement of the properties of such metallic corrosion-protecting coatings on rolled aluminium absorber plates. An antireflection (AR) layer is sometimes used to improve the efficiency of an absorbing surface. Chen *et al.* [5] has done work involving the development of AR coatings on plastic panels for display applications and Nostel *et al.* [6] also did some work involving the development of AR coatings. The coatings can be made on glass or metal plates.

Several techniques can be used to produce coatings on metallic plates. These can be divided into wet-chemical, paint, and vacuum deposition techniques. In general, the wet chemical approaches such as the sol-gel technique, have been the most widely used techniques for low temperature solar absorber applications. Katumba *et al.* [7], Haddad *et al.* [8] and Mackenzie *et al.* [9] have used the sol-gel technique to prepare coating for different applications.

1.2. Objectives of the study

This thesis deals with selective solar absorber surfaces, which are of the absorber-reflector tandem type [7], obtained by the sol-gel technique. Two kinds of materials have been studied. Sol-gel fabricated composite coatings of carbon nanoparticles embedded in nickel oxide (C-NiO) and in silica (C-SiO₂) on aluminium and stainless steel substrates have been used in the work reported here. The sol-gel technique was used because it affords easier control of coating

parameters such as particle size, distribution, homogeneity and film thickness [10]. It also offers the opportunity to adapt and utilise industrial applications such as spray-painting that are already in use for large surface area coatings.

The experimental work can be divided into two main parts. These are sample preparation and characterization. The sample preparation involved cleaning aluminium and steel substrates, mixing the chemicals in desired compositions, spin coating and heat-treating the coated substrates. After heat treatment the samples were ready for optical characterization. Hemispherical reflectance measurements were done using the Shimadzu UV/Vis/NIR LISR-3101 and the Buck M500 IR spectrophotometers. Different variables were investigated for each material.

C-NiO samples were prepared by dissolving nickel acetate in ethanol, adding diethanolamine (DEA), polyethylene glycol (PEG) and sucrose solution. A similar method of preparation has been used by Liu *et al.* [11]. The solution was then coated on clean substrates. The dependence of sucrose and PEG content on reflectance was investigated independently. The reflectance of coatings done at different speeds was also investigated. The thickness of the substrates coated at a given speed was measured since the sample properties depend on it. The main variable investigated was the annealing temperature since it affects the working temperature of the solar absorbers.

C-SiO₂ samples were prepared by mixing tetraethyl orthosilicate (TEOS) with acidified sucrose solution and adding methyl trimethoxysilane (MTES). This method has been used by

Katumba *et al.* [7]. The samples were heated at different temperatures to investigate the dependence of reflectance on annealing temperature.

1.3. Scope of the study

This dissertation is divided into five chapters. Chapter 1 introduces the subject and objectives of the work. Chapter 2 contains the theoretical background on the utilisation of solar thermal energy. This Chapter also contains the principles of operation of a solar collector and of a spectrally selective absorber surface. Some generally used absorber design principles are briefly described. The modelling (engineering) of optical constants using two well-known models, the Bruggeman and Maxwell Garnet effective medium approximations are also discussed in this Chapter. Another model called the Ping Sheng is discussed in brief. This chapter also communicates the chemistry involved in the sol-gel manufacturing method and the Michelson interferometry technique of film thickness measurement. The procedure followed in the preparation of coatings and in the optical characterisation is discussed in Chapter 3. Chapter 4 contains the main results for all the characterisation and their discussion. Chapter 5 contains conclusions and recommendations.

CHAPTER 2. THEORETICAL BACKGROUND

2.1 Introduction

This chapter gives the theoretical background necessary to understand this work on spectrally selective solar absorbers. A knowledge of the electromagnetic phenomena helps to understand solar and thermal radiation. The purpose of the solar absorber is to absorb the radiation from the sun and retain the heat. This heat is then used in different applications. The fabrication of solar absorber coatings must be cost effective and environmentally friendly.

2.2. Electromagnetic radiation

J. C. Maxwell discovered that electromagnetic radiation is a propagating wave with electric and magnetic components [12]. These components oscillate at right angles to each other and to the direction of propagation. Generally, electromagnetic radiation is classified by wavelength (or frequency) into radio, microwave, infrared (IR), visible region (Vis), ultraviolet (UV), X-rays and gamma (γ) rays. The wavelengths of interest in many applications utilizing solar radiation are found in the UV to IR range (0.3 to 50 μ m) [2]. This range includes the solar spectral range and the thermal range. The solar spectral range (UV/Vis/NIR) has wavelengths ranging from 0.3 to 2.5 μ m and the thermal range ranges from 2.5 to 50 μ m. An ideal solar absorber would have 100 % absorptance in the solar spectral range and 0 % emittance in the thermal range.

2.2.1. Solar radiation

When the sun's rays are passing through the earth's atmosphere, a portion of solar radiation is scattered by air molecules, water vapour and dust particles. The portion that reaches the earth's surface direct from the sun is called direct radiation. That which is scattered reaches the earth's

surface as either diffuse or reflected radiation. The total intensity of solar radiation falling on the earth is the sum of the direct radiation, I_D , diffuse radiation, I_d , and reflected radiation, I_{ref} .

$$I_t = I_D + I_d + I_{ref}$$
 (2.1)

Figure 2.1 shows the solar hemispherical spectral irradiance for air mass 1.5 (ISO, 1992) and the blackbody spectral emittance at different temperatures.

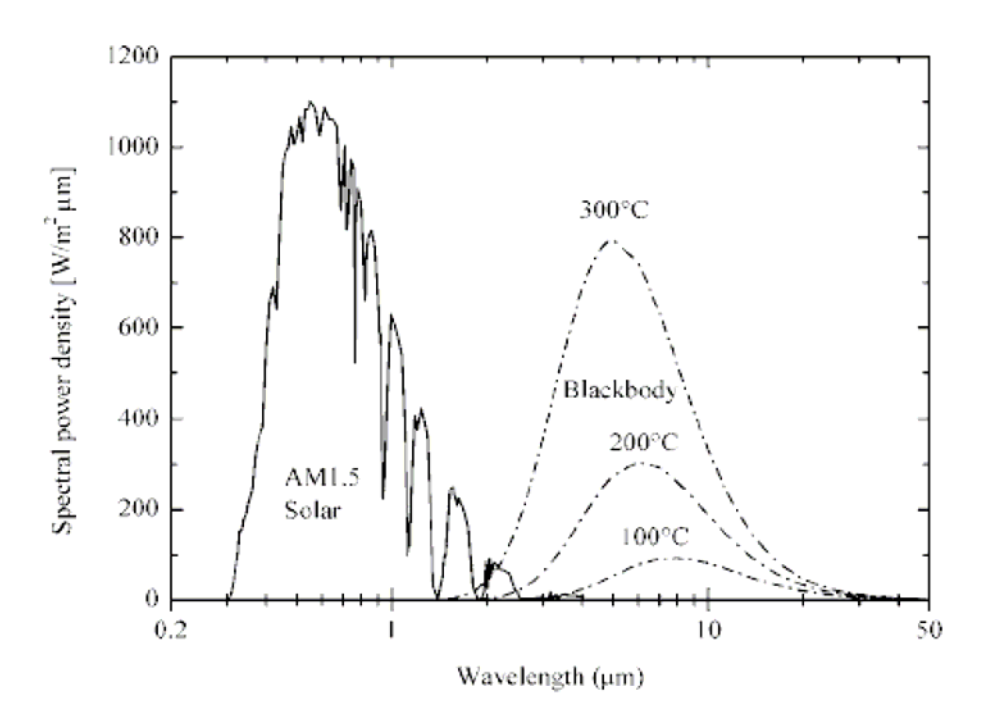


Figure 2.1. Solar hemispherical spectral irradiance for air mass 1.5 (ISO, 1992) and blackbody spectral emittance at 100 °C, 200 °C and 300 °C. Adapted from Konttinen [13].

2.2.2. Thermal radiation

All heated bodies emit thermal electromagnetic radiation whose wavelength and intensity are dependent on the temperature of the body and its optical characteristics. A blackbody is defined as an ideal body that allows all the incident radiation to pass into it and internally absorbs all the incident radiation [14]. This is true of radiation for all wavelengths and for all angles of incidence. The blackbody also emits the maximum radiant energy. As a perfect absorber, it serves as a standard with which real absorbers can be compared. As a perfect emitter, it serves as an ideal standard of comparison with a real body emitting radiation. The blackbody spectral emittance at different temperatures is shown in Figure 2.1.

Plank's law [15] of blackbody radiation gives the spectral intensity, E_b , of electromagnetic radiation from a blackbody at temperature, T as:

$$E_{\lambda b} = \frac{2\pi h c^2}{\lambda^5} \left[\frac{1}{e^{hc/\lambda kT} - 1} \right]. \tag{2.2}$$

where $E_{\lambda b}$, the spectral intensity is in W m⁻³ sr⁻¹, h is the Plank's constant in J s⁻¹, c is the speed of light in vacuum in m s⁻¹, λ is the wavelength of the radiation in metres, c is the Boltzmann constant in J K⁻¹. The groups $2\pi hc^2$ and hc/k are often called Plank's first and second radiation constants and are given the symbols C_1 and C_2 respectively. Recommended values are $C_1 = 3.7405 \times 10^{-1}$ m² W and $C_2 = 0.0143879$ m K.

The total emitted energy can be obtained by integrating the Plank's law (equation 2.2) over the whole wavelength range.

The Stefan-Boltzmann law [2-4,13-15] states that the total energy radiated per unit surface area of a black body in unit time (irradiance), E_b , is directly proportional to the fourth power of the body's thermodynamic temperature, T. This is found from integrating Plank's law over all wavelengths.

$$E_b = \int_0^\infty E_{\lambda b} d\lambda = \sigma T^4 \tag{2.3}$$

where $\sigma = 5.669 \text{ 7} \times 10^{-8} \text{ W m}^{-2} \text{ K}^{-4}$ is the theoretical Stefan-Boltzmann constant [15].

2.2.3. Radiation Tables

Starting with the Plank's law of the spectral distribution of blackbody radiation, Dunkle [16] has presented a method for simplifying blackbody radiation calculations. Equation 2.2 can be integrated to give the radiation between any limits. The total radiation emitted from zero to any wavelength, λ , is given by:

$$E_{0-\lambda,b} = \int_{0}^{\lambda} E_{\lambda b} d\lambda \tag{2.4}$$

Substituting equation (2.2) into equation (2.4) and noting that if equation (2.4) is divided by σT^4 , the integral can be made to be only a function of λT ,

$$f_{0-\lambda T} = \frac{E_{0-\lambda T,b}}{\sigma T^4} = \int_0^{\lambda T} \frac{C_1 d(\lambda T)}{\sigma(\lambda T)^5 \left[\exp(C_2 / \lambda T) - 1\right]}$$
(2.5)

The value of this integral is the fraction of the blackbody energy between zero and λT . The values calculated by Sargent [17] for convenient intervals are given in Tables C1 and C2 in Appendix C. When the upper limit of the integration is infinity, the value of the integral is unity.

2.3. Solar collectors

Solar collectors transform solar radiation into heat and transfer that heat to a medium (water or any other fluid used). The solar heat can be used for heating the fluid. The heart of the solar collector is the solar absorber, which is usually composed of several narrow metal strips. The solar absorber is in contact with conduit pipes that carry the fluid responsible for transferring the heat. Absorbers are usually black since black surfaces have a high degree of light absorption. In order to reduce energy loss through heat emission, the most efficient absorbers have a selective surface coating. This coating enables the conversion of a high proportion of the solar radiation into heat while reducing the emission of heat.

There are three main types of solar collectors, which can be used in active solar heating systems. These are: evacuated tubes, flat plate collectors and unglazed plastic collectors. The samples studied here are mainly suitable for use as flat plate solar collectors. The structure of a flat plate collector is described in Section 2.3.1.

2.3.1. Flat plate solar collectors

The cross-sectional view of a simple flat plate collector used for domestic hot water applications is shown in Figure. 2.2.

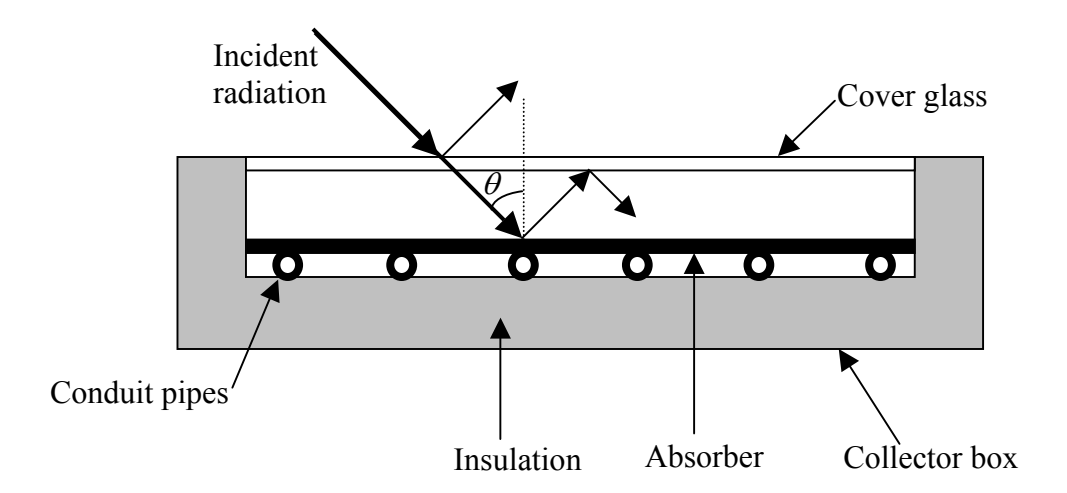


Figure 2.2. Cross-sectional view of a flat plate solar collector design used for domestic hot water applications.

It consists of a frame, a transparent top glass cover, insulation, and an absorber as shown above. Usually an iron-poor solar safety glass is used as a transparent cover, as it transmits a great amount of the short-wave light spectrum. The glass cover allows only very little of the heat emitted by the absorber to escape out of the collector (greenhouse effect). The transparent cover also helps to prevent wind and breezes from carrying the collected heat away (convection). Together with the frame, the cover protects the absorber from adverse weather conditions. Typical frame materials include aluminium and galvanized steel. Fibre-glass-reinforced plastic is sometimes used as a frame material [5].

The insulation on the back of the absorber and on the sidewalls reduces the heat loss through conduction. In order to reduce heat loss within the frame by convection, the air can be pumped out of the collector tubes. Such collectors are called evacuated-tube collectors. They are usually re-evacuated after every few years. This is because when the temperature is high some gases can be released from the reactions taking place at the absorber surface.

The collector efficiency, η , is defined as the ratio between the power output from the collector, Q_u , and the incident solar power:

$$\eta = \frac{Q_u}{A_c G_T} \tag{2.6}$$

where A_c is the collector area and G_T is the total incident solar energy flux. The power output from the collector depends on the thermal energy losses from the collector. The energy lost to the surroundings due to convection, conduction and thermal radiation is described as the over all collector heat transfer coefficient, U_L times the difference between the absorber plate temperature, $T_{p,m}$ and the ambient temperature, T_a :

$$Q_{u} = A_{c}[(\tau \alpha)_{eff} G_{T} - U_{L}(T_{p,m} - T_{a})]$$
(2.7)

where $(\tau \alpha)_{eff}$ is the effective transmittance-absorptance product. The amount of solar radiation in the solar absorber plate is implicitly included in the term $(\tau \alpha)_{eff}$ and the amount of thermal radiation losses from the absorber plate is included in U_L .

A theory behind the fabrication method used in this work will now be discussed.

2.4. Fabrication of spectrally selective solar absorber coatings

There is a variety of techniques used in the fabrication of solar absorber coatings. These are sputtering [4], sol-gel process [7-11,18-32], chemical vapour deposition (CVD), electroplating, anodization, mechanical grinding [13,33-39], inorganic pigmentation of anodised aluminium, and physical vapour deposition (PVD).

2.4.1. Introduction to the sol-gel technique

The sol-gel process is the one used to synthesize thin film coatings in the work being reported here. Its most important advantage over conventional thin film forming processes such as CVD, electroplating and sputtering is that it offers the ability to control precisely the microstructure of the deposited film, i.e., the absorber particle size, particle size distribution, homogeneity and thickness [7,18]. The other advantage is that it is less expensive since it requires less equipment than the other methods.

The sol-gel process can be divided into a number of steps. These are: preparation of precursor solutions (sols), deposition of the sols onto glass, plastic or metal substrates and drying. Preparation of sols involves hydrolysis and polymerisation of alkoxides like tetraethyl orthosilicate (TEOS) [19]. Common deposition processes are dip coating, spraying or spin coating [1,18,20]. A detailed discussion of the spin coating method is given in section 2.4.4.

2.4.2. The chemistry of the sol-gel technique

In the sol-gel process, the precursors for preparation of a colloid (sol) consist of a metal or metalloid element surrounded by various ligands (appendages not including another metal or metalloid atom). Sol differs from a solution in that a solution is a single-phase system, while a sol

is a suspension of small particles of one phase in another major (usually liquid) phase. The most popular precursors are metal alkoxides [18]. The reason being that they react readily with water. This type of reaction is called hydrolysis. In hydrolysis a hydroxyl ion becomes attached to the metal atom, as in reaction (2.8).

$$Si(OR)_4 + H_2O \rightarrow HO - Si(OR)_3 + ROH$$
 (2.8)

The R represents a proton or other ligand (if R is an alkyl, then $\cdot OH$ is an alkoxy group), and ROH is an alcohol.

Depending on the amount of water and catalyst present, hydrolysis may go to completion (so that all of the *OR* groups are replaced by *OH*):

$$Si(OR)_4 + 4H_2O \rightarrow Si(OH)_4 + 4ROH \tag{2.9}$$

or stop while the metal is only partially hydrolysed to give $Si(OR)_{4-n}(OH)_n$. Inorganic precursors can also be hydrolysed. Two partially hydrolysed molecules can link together in a condensation reaction, such as (2.10).

$$(OR)_3 Si - OH + HO - Si(OR)_3 \rightarrow (OR)_3 Si - O - Si(OR)_3 + H_2O$$
 (2.10)

or

$$(OR)_3 Si - OR + HO - Si(OR)_3 \rightarrow (OR)_3 Si - O - Si(OR)_3 + ROH$$
(2.11)

Condensation liberates a small molecule, such as water or alcohol. This type of reaction can continue to build larger and larger molecules containing silicon by the process of polymerisation. A polymer is a huge molecule (also called a macromolecule) formed from hundreds of thousands of units called monomers that are capable of forming at least two bonds.

If a monomer can make more than two bonds, then there is no limit on the size of the molecule that can form. If one molecule reaches macroscopic dimensions so that it extends throughout the solution, the substance if called a gel. Rabinovich [21] defines a gel as a solid, usually soft and with low elastic modulus. It may not differ from the parent sol in its composition and solid/liquid ratio or it may expulse part of the liquid and appear to be immersed in this liquid. The gel point is the time at which the last bond is formed that completes this giant molecule. Thus a gel is a substance that contains a continuous solid skeleton enclosing a continuous liquid phase. The continuity of the solid structure gives elasticity to the gel. If a sol does not gel, it usually is as stable as a solution. A sol may not gel because of the small size of the dispersed phase, which results in negligible gravitational forces.

Bond formation continues at the gel point. Segments of the gel network continue to move close enough together to allow further condensation and other bond forming processes. The smaller polymers or particles continue to attach themselves to the network. The term aging is applied to the process of change in structure and properties after gelation.

Preparation of thin films is by far the most important use of sols and gels. Other uses of sols and gels are given by Brinker and Scherer [22].

2.4.3. The sol-gel coating process

The sol-gel coating process usually consists of four steps:

- 1) preparation of the sol (colloidal particles dispersed in a liquid)
- 2) deposition of sol solution on substrates to produce coatings.
- 3) polymerization of the particles in the sol through the removal of stabilizing components and formation of a gel in a state of a continuous network.
- 4) drying to pyrolyze the organic and inorganic components to form an amorphous or crystalline coating.

The chemistry of the sol-gel technique has been discussed in Section 2.4.2. Knowledge of the chemical processes taking place when mixing up chemicals can enable someone to prepare a sol that gels. The next section will discuss one of the deposition techniques used to apply the sol onto substrates.

2.4.4. The spin-coating deposition technique

Spin coating is a quick and convenient method for the preparation of sol-gel coatings. An illustration of the spin coating process is shown in Figure 2.3.

The substrate is placed on top of a chuck that is driven by a motor. The liquid or sol is applied from a suitable dispenser, such as a syringe.

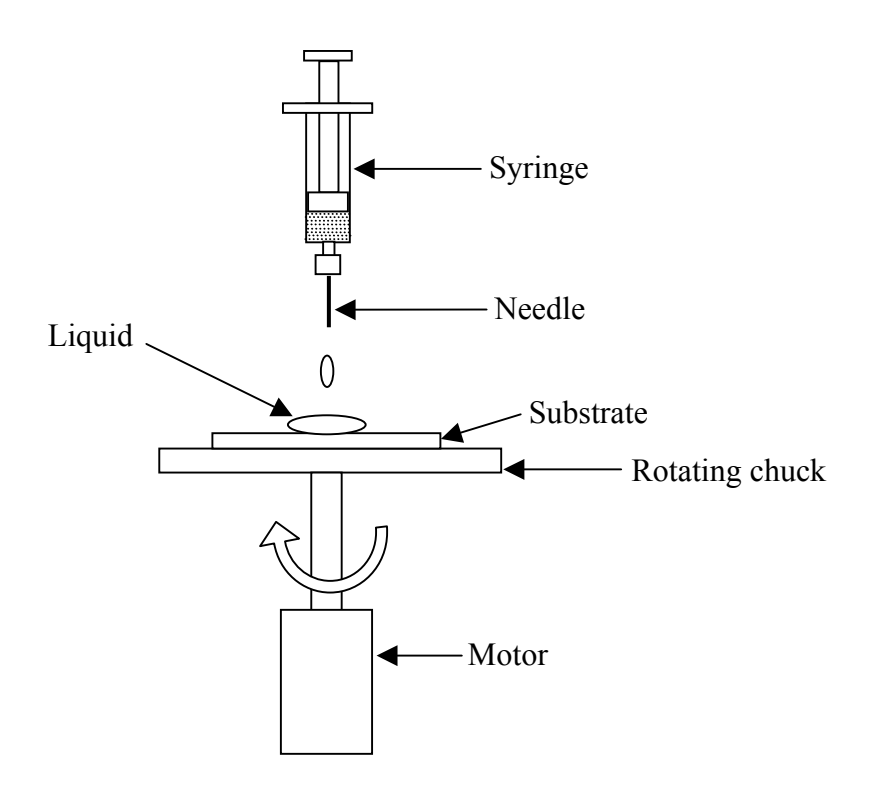


Figure 2.3. Illustration of the spin coating process.

There are basically three steps to the spin coating process. In the first, a substantial excess of coating solution is applied to the substrate. The substrate can be at rest, rotating slowly or at speed. In the second stage, the coating solution moves radially outwards from the centre driven by the centrifugal force generated by the rotating chuck. The surface of the chuck is flooded with the coating solution and the excess is thrown off the edges. After the spinning, the substrate will be coated with a film of uniform thickness. In the third stage, the liquid film solidifies, usually by solvent evaporation or in many sol-gel systems, by gelation.

Usually after these processes, a uniform thin coating is obtained. However, complications can easily arise. Viscosity and temperature changes can arise during the process to give rise to inhomogeneities in the coating. Viscosity changes are a result of using solvents with lower

boiling temperatures. Trying to eliminate this problem using higher boiling point solvents sometimes cause trouble because the film becomes overly thin. Besides viscosity and temperature changes, the other variable that can affect the quality of the final film is the tension.

Two forces dominate spin coating. These are the centrifugal force, which drives the liquid outwards, and the resisting viscous force, which acts radially inwards. In an ideal system the coating thickness is inversely proportional to the square root of the rotation speed [23,24]:

$$thickness = \left[\frac{1}{speed}\right]^{1/2}.$$
 (2.12)

In a real situation the film thickness is further reduced due to solvent evaporation, which leads to gelation or solidification when the concentration reaches a certain level. After this process the coatings may be heat-treated. The operation of the spin coater used in the department of Physics of the University of Zimbabwe is described by Makiwa [40].

2.4.5. Heat treatment of coatings

It can be learnt from Section 3.2.1 that the gel is a wet body. The drying of the gel is a process of removing liquid particles from the tiny pores. Unfortunately this is not an easy job since it causes significant stress resulting from inhomogeneous shrinkage. In some cases this stress causes samples to develop cracks. Brinker and Scherer [23] describe the stages of drying as:

1. Constant rate period. This is when the decrease in volume of the gel is equal to the volume of liquid lost by evaporation.

- 2. Critical point. The end of the first stage when shrinkage stops and cracking is most likely to occur.
- 3. First falling rate period. The process of liquid flow through partially empty pores.
- 4. Second falling rate period. The final stage of drying, when the liquid can escape only by diffusion of its vapour to the surface.

Cracking occurs when the stress in the network exceeds its strength. Methods that reduce or eliminate cracks include aging, chemical additives and supercritical drying.

Samples can also be heat treated to test the coating's applicability in concentrating solar power (CSP) applications. They must be stable at temperature above 400 °C in order work in these high temperature environments. After the heat treatment the samples are characterized.

2.5. Spectrally selective solar absorbing surfaces

2.5.1. Solar absorptance and thermal emittance of spectrally selective solar absorbers

A spectrally selective absorber has different spectral reflectance at different wavelengths. The ideal spectrally selective surface operating below 100 °C has a zero reflectance (100% absorptance) in the 0.3 to 2.5 μm range and 100% reflectance (0% solar absorptance) in the 2.5 to 50 μm range. Unfortunately such an ideal surface does not exist in nature. It is the purpose of this work to fabricate a material that is close to this ideal behaviour as shown in Figure 2.4. In order to evaluate absorber surface behaviour, one has to know the blackbody spectrum at a given temperature and the spectral distribution of the sun. After absorption in the atmosphere, the standard spectral solar flux incident at the earth's surface is in the 0.3 to 2.5μm wavelength

The solar irradiance that reaches the earth's surface during a clear sky with a dry

atmosphere is shown in Fig 2.1. This is adapted from the International Organisation for Standardization (ISO) for air mass 1.5 (AM1.5) i.e. when the sun is about 42 ° above the horizon [2]. Both direct and diffuse radiation (Section 2.2.1.) contained in the spectrum contribute to the heating-up of flat plate solar collectors.

When the temperature of the blackbody increases (Fig 2.1.) the amount of the emitted energy increases and the location of the peak power density shifts towards shorter wavelengths. The peak wavelength can be determined from the Wien's displacement law, equation (2.8) [15]. The peak wavelength is derived by differentiating Plank's wavelength distribution law, equation 2.2 and equating it to zero.

$$\lambda_{\text{max}}T = 2897.8 \ \mu \text{ m K}.$$
 (2.13)

where the constant 2897.8 μ m K is known as Wien's constant [41].

When radiation strikes a body, a part of it is reflected, a part is absorbed, and if the material is transparent, a part is also transmitted. Commonly quoted parameters of performance for selective surfaces are the angle-dependent solar absorptance, $\alpha(\lambda, \theta)$, and hemispherical thermal emittance, $\varepsilon(\lambda, \theta)$. The solar absorptance is defined as a weighted fraction of the intensity of incident radiation that is absorbed at a specific wavelength, λ and angle of incidence, θ [4]. Emittance, is the ratio of the intensity of emitted radiation and that emitted by a blackbody at the same wavelength and temperature. The fraction that is reflected is called reflectance, $R(\lambda, \theta)$ and the fraction that is transmitted is transmittance, $T(\lambda, \theta)$. When determining the absorptance or the emittance of a material, it is usually most convenient to first measure the reflectance and to

calculate the other two parameters from it. This is true only for opaque samples; otherwise one needs at least two measurements to determine the third parameter.

From the principle of conservation of energy:

$$\alpha(\lambda,\theta) + R(\lambda,\theta) + T(\lambda,\theta) = 1. \tag{2.14}$$

Kirchhoff's law states that at a given wavelength, the absorptance is equal to the emittance for matter in thermodynamic equilibrium [15] i.e.

$$\varepsilon(\lambda,\theta) = A(\lambda,\theta). \tag{2.15}$$

Equation (2.7) can now be written as:

$$\varepsilon(\lambda,\theta) = A(\lambda,\theta) = 1 - R(\lambda,\theta) - T(\lambda,\theta). \tag{2.16}$$

For an opaque material the transmittance $T(\lambda, \theta)$ is equal to zero. Spectral absorptance can be expressed in terms of the total reflectance $R(\lambda, \theta)$, as:

$$\alpha_{sol}(\lambda,\theta) = 1 - R(\lambda,\theta) \tag{2.17}$$

The angle-dependent solar absorptance, $\alpha_{sol}(\theta)$, is found by weighing the spectral absorptance with the spectral solar irradiance, $I_{sol}(\lambda)$, and can be obtained by integrating over the wavelength dependent spectrum to give:

$$\alpha_{sol}(\theta) = \frac{\int_{\lambda_{1}}^{\lambda_{2}} I_{sol}(\lambda)(1 - R(\lambda, \theta))d(\lambda)}{\int_{\lambda_{1}}^{\lambda_{2}} I_{sol}(\lambda)d(\lambda)}$$
(2.18)

where λ_1 and λ_2 are the lower and upper solar wavelengths respectively.

The hemispherical thermal emittance, $\varepsilon_{therm}(\theta, T)$, is defined as the ratio of emitted radiation to that of a blackbody at a given temperature and is given by:

$$\varepsilon_{therm}(\theta, T) = \frac{\int_{0}^{\pi/2} \sin 2\theta d\theta \int_{\lambda_{3}}^{\lambda_{4}} I_{P}(\lambda, T)(1 - R(\lambda, \theta))d(\lambda)}{\int_{\lambda_{3}}^{\lambda_{4}} I_{P}(\lambda, T)d(\lambda)}$$
(2.19)

where $I_P(\lambda, T)$ is the spectral blackbody emissive power.

The total near-normal ($\theta = 0^{\circ}$) solar absorptance, $\alpha_{sol}(\theta)$ and total hemispherical thermal emittance, ε_{therm} , are then respectively given by:

$$\alpha_{sol} = \frac{\int_{\lambda_1}^{\lambda_2} I_{sol}(\lambda)(1 - R(\lambda))d(\lambda)}{\int_{\lambda_1}^{\lambda_2} I_{sol}(\lambda)d(\lambda)}$$
(2.20)

and

$$\varepsilon_{therm} = \frac{\int_{\lambda_1}^{\lambda_2} I_B(\lambda)(1 - R(\lambda))d(\lambda)}{\int_{\lambda_1}^{\lambda_2} I_B(\lambda)d(\lambda)}$$
(2.21)

The selected ordinate formula performed in the wavelength range of 5 to 50 µm:

$$\varepsilon_{therm} = \frac{1}{30} \sum_{i=1}^{30} 1 - R(\lambda) \tag{2.22}$$

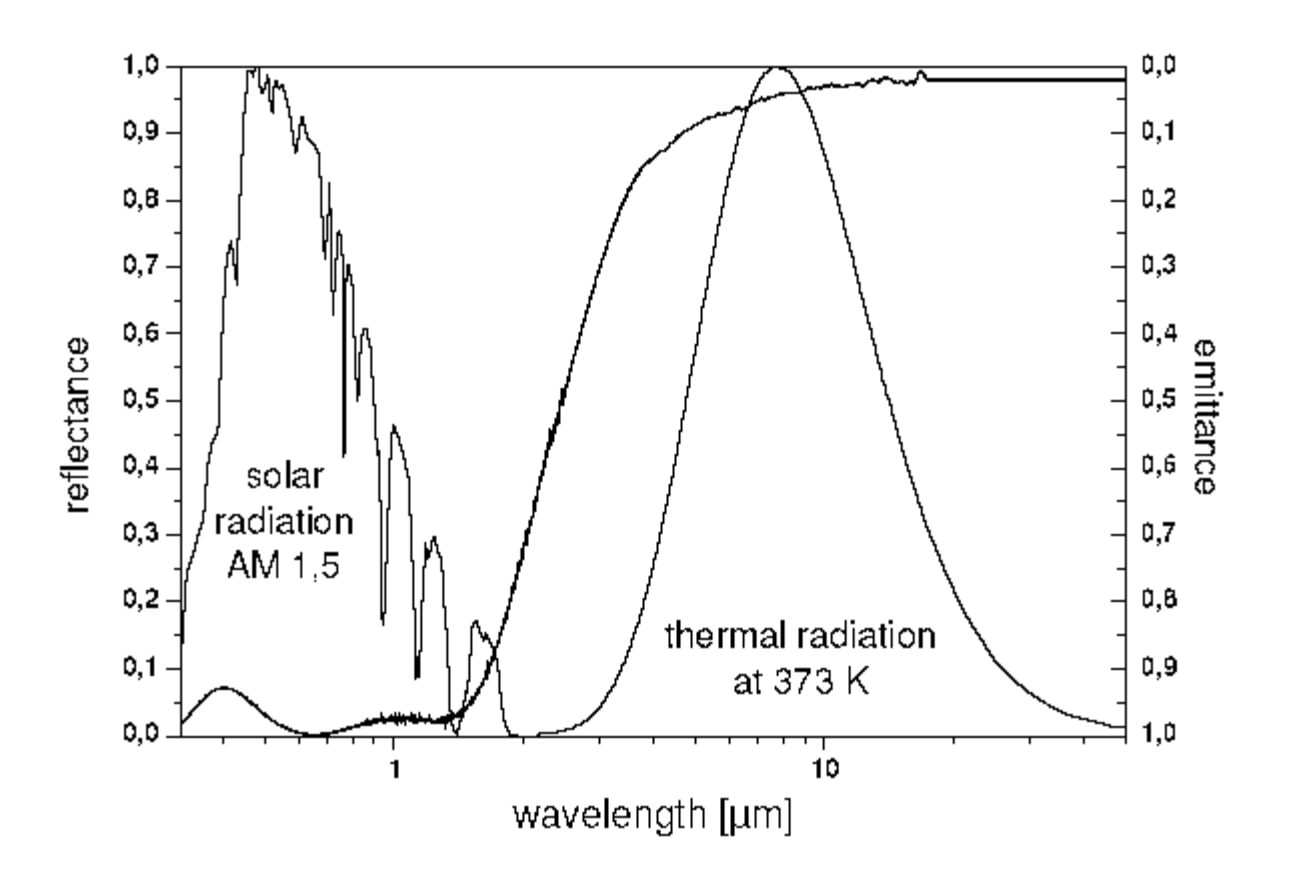
is used to calculate the numerical value for the thermal emittance. This is the European standard [42].

The photo-thermal conversion efficiency, h, can be calculated using the formula:

$$h = a_{sol} - \frac{\varepsilon_{therm} \ sT^4}{cI}$$
 (2.23)

where *s*, *T*, *c*, and *I* are Stefan-Boltzmann constant, operating temperature, flux amplification or concentration factor, and solar flux intensity respectively.

The reflectance and emittance of a typical spectrally selective solar absorber adapted from an unspecified source is given in Figure 2.4. The solar absorber has a solar absorptance of 96.1% and a thermal emittance of 5.2%.



Solar absorptance (AM1.5) = 96.1 %

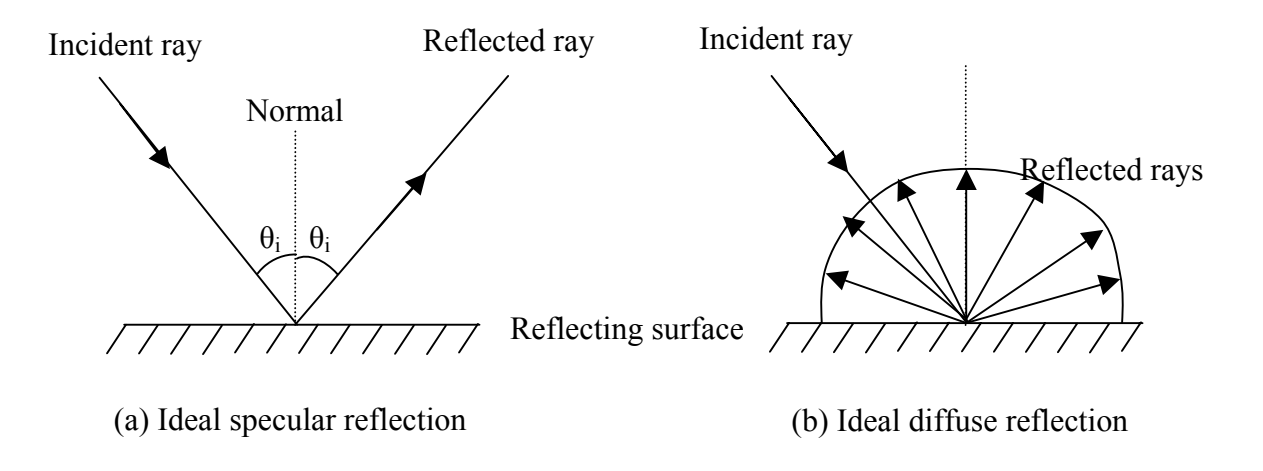
Thermal emittance (373K) = 5.2 %

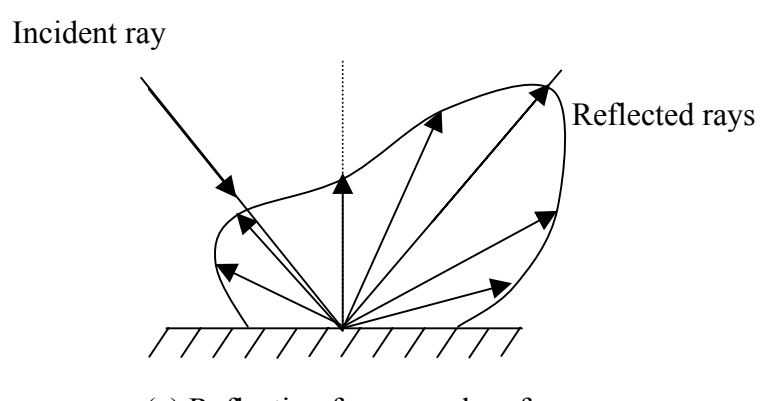
Figure 2.4. Solar absorptance and thermal emittance of a typical commercial spectrally selective solar absorber. Adapted from an unspecified source.

2.5.1.1. Reflectance of spectrally selective solar absorber surfaces

Reflection of radiation can be specular or diffuse. Specular reflection is the mirror-like reflection of radiation from a surface, in which radiation from a single incoming direction is reflected onto a single outgoing direction with equal angles of incidence and reflection. This is in contrast to diffuse reflection in which incoming light is reflected in all directions equally. In practice, the reflection from a surface is both specular and diffuse. A highly polished surface approaches specular diffusion whereas a rough surface reflects diffusely.

Figure 2.5. illustrates ideal specular reflection, ideal diffuse (Lambertian) reflection and reflection from an ideal opaque surface.





(c) Reflection from a real surface

Figure 2.5. Reflection from ideal and real opaque surfaces.

Many optical instruments designed to measure reflectance can only measure specular reflection. To be able to measure diffuse reflection these instruments must be fitted with integrating spheres, which are coated with a completely diffuse, and highly reflecting surface.

2.5.2. Designs of spectrally selective solar absorbers

Selective solar absorbers have different designs depending on their operational temperature and applications. In principle there are several ways of achieving selective solar absorbing surfaces. Kennedy [3] and Niklasson *et al.* [43] categorized selective absorber surface coatings into six distinct types. These are:

- a) intrinsic;
- b) semiconductor-metal tandem;
- c) multilayer absorber;
- d) multi-dielectric composite coating;
- e) textured surfaces and
- f) selectively solar-transmitting coating on a blackbody-like absorber.

A detailed description of the different designs is given in the following subsections.

2.5.2.1. Intrinsic absorber

Intrinsic absorbers consist of a single material having intrinsic properties that result in a natural spectral selectivity. There are some materials in nature that have moderate selectivity. Various semiconductors or transition metals show selective characteristics but no material has been found to be sufficiently selective for spectrally selective applications. The problem with intrinsic absorbers is that the crossover from low to high reflectance occurs at too short wavelengths or that the slope at the transition wavelength is not sufficiently steep. Research in intrinsic

absorbers has therefore not been very productive. The structure of intrinsic absorbers is shown in Figure 2.6.



Figure 2.6. Schematic design of an intrinsic absorber.

G. Pellegrini [44] and E. Randrich *et al.* [45] have investigated CaF₂ and ZrB₂ intrinsic absorbers respectively. In practice useful absorbers are based on two or more layers with different optical properties. Such devices are called absorber reflector tandems. A dielectric or semiconducting coating with high solar absorptance and high infrared transmittance on top of a non-selective highly reflecting metal constitute the tandem absorber.

2.5.2.2. Semiconductor-metal tandem

Spectrally selective semiconductor coatings can be obtained by depositing a semiconductor, which has a low band gap so that it absorbs the solar radiation, on a highly infrared reflecting metal substrate. Figure. 2.7 shows the structure of a semiconductor-metal tandem absorber.

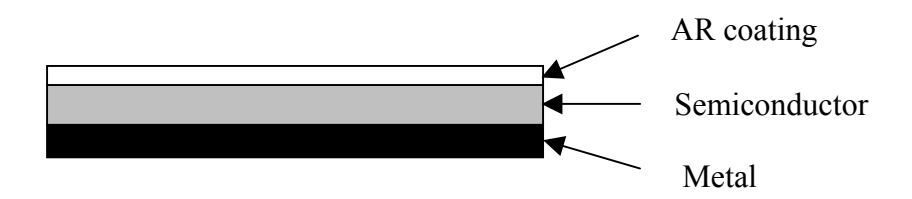


Figure 2.7. Schematic design of a semiconductor-metal tandem absorber.

The semiconductor coating absorbs photons having energies greater than the band gap as a result of raising the material's valence electrons into the conduction band. Photons with energies less than the band gap energy are transmitted through the coating unaffected. To obtain high solar absorptance, the refractive index of the semiconductor should be as low as possible. Unfortunately, semiconductor coatings have high refractive indices, which gives high reflectance at the semiconductor-air interface. The reflectance can be reduced through proper thickness control to obtain a destructive interference interface effect or by applying AR coatings [5].

Seraphin [46] has investigated SiO₂/Si₃N₄/Si/CrO₃/Ag/CrO₃ semiconductor coatings on steel and obtained encouraging results. The solar absorption achieved was 0.85 and the thermal emittance was 0.07 at 500^oC. However, the low mechanical strength, low thermal conductivity and high cost of semiconductors make them unsuitable for the entire collector material [47].

2.5.2.3. Multilayer absorber

A multilayer absorber consists of several alternating layers of dielectric and semi-transparent metallic materials. An AR layer is often put on top. The schematic diagram of a multilayer absorber is shown in Figure 2.8.

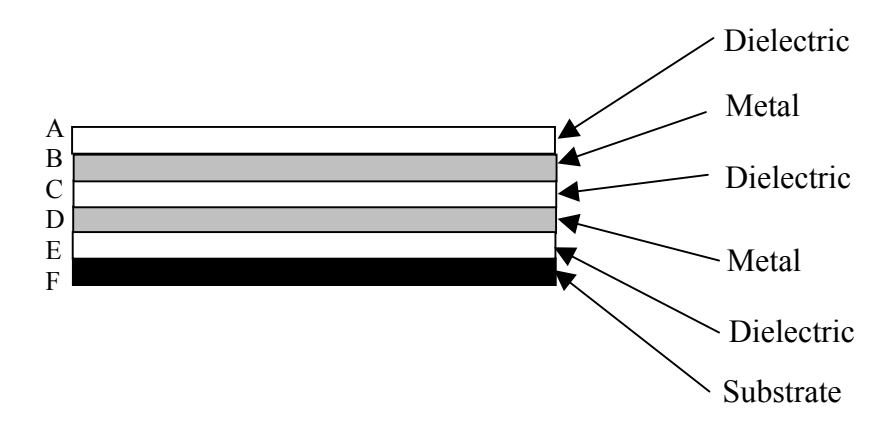


Figure 2.8. Schematic design of a multilayer absorber.

A thin semitransparent reflective metallic layer D separates two quarter-wave dielectric layers, C and E. The bottom reflecting layer D has high reflectance in the IR region and is slightly less reflective in the visible region. The thickness of this dielectric determines the shape and position of the reflectance curve. An additional semitransparent thin metallic layer B further reduces the reflection in the visible region, and an additional dielectric layer A increases the absorption in the visible region and broadens the region of high absorption. One interesting example of multilayer absorber is the Al₂O₃/Mo/Al₂O₃, which has been produced by large area sputtering technology [43].

2.5.2.4. Metal-dielectric composite

A metal-dielectric or cermet absorber consists of metal particles embedded in a dielectric matrix deposited on a highly infrared reflecting metal substrate. The particles are usually transition metals embedded in an oxide matrix. Figure. 2.9 shows the structure of a metal-dielectric composite.

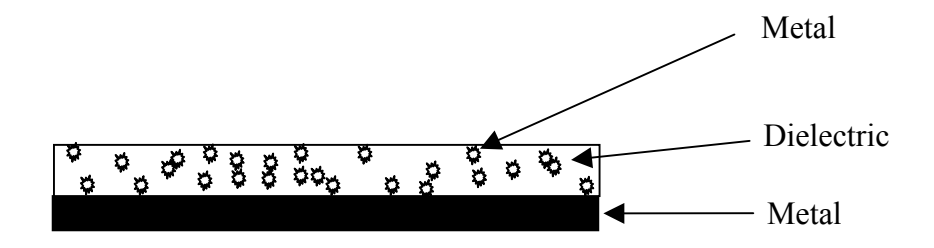


Figure. 2.9. Schematic design of a metal-dielectric absorber.

The metal-dielectric concept offers a high degree of flexibility because the solar selectivity can be optimised by proper choice of constituents, coating thickness, particle concentration, size, shape and orientation. The solar absorptance can be boosted by a suitable choice of substrates, and AR layers. The composite coatings can be produced by a variety of techniques such as electroplating, anodization, inorganic colouration of anodized aluminium, chemical vapour deposition (CVD) and co-deposition of metal and insulator by evaporation and sputtering.

2.5.2.5. Textured surfaces

These are produced by creating texture of suitable scale on a highly reflecting metal substrate like aluminium, copper or steel. Textured surfaces can produce high solar absorptance by multiple reflections among needle-like, dendritic, or porous microstructure. For long wavelength radiation, the surface looks fairly smooth thereby acting like a poor radiator of thermal energy (low ε_{therm}). Figure 2.10 shows the structure of a textured surface absorber. Well known examples are dendritic tungsten prepared by CVD.

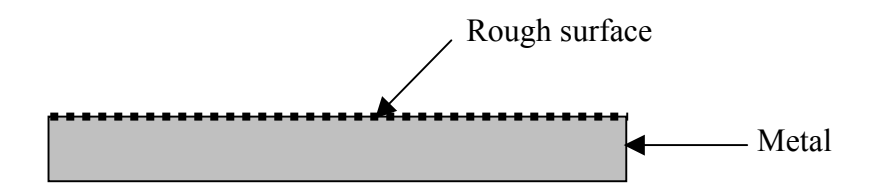


Figure 2.10. Schematic design of a surface textured solar absorber.

2.5.2.6. Solar transmitting coating/blackbody-like absorber

A solar transmitting coating can be made by depositing a highly doped semiconductor like SnO₂:F or ZnO:Al over an absorber with a proven long-term durability. Some low-temp flat-plate collectors have used black enamel as the absorber material [3]. Figure 2.11. shows the schematic diagram of a solar transmitting coating.

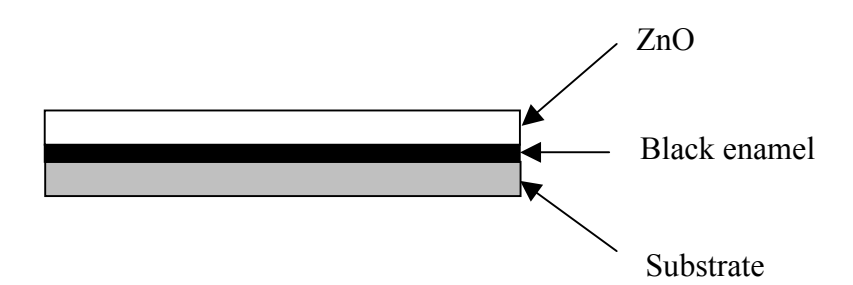


Figure 2.11. Schematic diagram of a solar transmitting coating.

2.5.2.7. Selective solar paint coatings

Selective solar absorbing paints have the potential of being a less expensive alternative to the selectively solar absorbing coatings described in Sections 2.4.2.1 to 2.4.2.6. They can also be classified as the tandem type of absorbing particles uniformly distributed in a matrix deposited on a metal substrate. Their optical performance is governed by intrinsic optical constants as well as

particle size dependent scattering and absorption. The combined effect gives the effective scattering and absorption coefficients of the pigments. Examples of solar absorbing paints that are on the market are Solarect-Z and SolkoteHI/SORB-IITM [2]. These are used for low temperature flat plate collectors.

2.5.3. Engineering of optical constants

An electromagnetic wave that propagates in a medium can be described by its electric and magnetic fields [4,48]. Equations (2.24) and (2.25) give the electric and magnetic field intensities (E and H) respectively.

$$E_m = E_o e^{-k\alpha x/c} e^{i(\omega t - n\alpha x/c)}$$
(2.24)

and

$$H_m = H_o e^{-k\alpha x/c} e^{i(\omega t - n\alpha x/c)}$$
(2.25)

where: E_m and H_m are the amplitudes at position x and time t after entering the medium;

: E_o and H_o are the maximum amplitudes;

: ω is the angular frequency;

: n and k are the real and imaginary part of the refractive index and

: *c* is the speed of light in vacuum.

It can be seen that changing the real part of the refractive index changes the phase velocity and changing the imaginary part changes the amplitude. Considering radiation in the UV to IR wavelength range, it is the electric field only that is affected.

Beer-Lambert's law [49] states that the intensity, I, of a beam of radiation propagating in a medium varies according to equation (2.26):

$$I = I_{o}e^{-\alpha x} \tag{2.26}$$

where I_o is the original intensity of beam before it enters the medium, x is the path length and α is the absorption coefficient. The absorption coefficient is related to the imaginary part of the refractive index by equation (2.27):

$$\alpha = \frac{2\omega k}{c} = \frac{4\pi k}{\lambda} \tag{2.27}$$

The absorbance, A, of a medium of thickness, d, is a measure of the logarithmic reduction of the intensity of the radiation as it passes through it:

$$A = -\log \frac{I}{I_0} = \alpha d = 4\pi \frac{kd}{\lambda}$$
 (2.28)

It is the factor $\frac{kd}{\lambda}$ that is important for the efficiency of a solar absorber coating. It determines where the crossover shown in Fig 2.4 occurs. The wavelength range where the crossover should be can be tailored by varying the combination of k and d. The only factor that can be changed for homogeneous media is the thickness, d. For composite films, k is the only factor that can be changed.

When considering materials normally used for selective solar absorber applications, k, is fairly constant and so the thickness, d, can be considered as the only factor that determines the position of the crossover.

The reflectance, R, at near-normal incidence for a bulk material is given by equation (2.29) [48, 50]:

$$R = \left| \frac{1 - N}{1 + N} \right|^2 \tag{2.29}$$

where N is the complex refractive index given by equation (2.30).

$$N = n + ik \tag{2.30}$$

As described earlier, n is the real part and k is the imaginary part of the refractive index. The complex refractive index, N, is related to the complex dielectric function, ε by:

$$\varepsilon = N^2 \tag{2.31}$$

The complex dielectric function, ε , consists of the real and imaginary parts, ε_1 and ε_2 respectively. These are related by equation (2.32):

$$\varepsilon = \varepsilon_1 + i\varepsilon_2 \tag{2.32}$$

Combining equations (2.30) to (2.32) gives:

$$\varepsilon_1 = n^2 - k^2 \tag{2.33}$$

and

$$\varepsilon_2 = 2nk \tag{2.34}$$

Using these equations, an expression to relate the reflection at near-normal incidence to the real and complex parts of the dielectric function can be derived. Bruggeman [51] proposed a model widely used for the dielectric function of a composite. A description of the model is given by Gelin [4] and Zhang [52]. Another model by Maxwell-Garnet [53] exists. It is described in detail by Nicklasson [43]. Tesfamichael [2] also described a third model called the Ping Sheng model. These three models can be used to model the effective dielectric function of a composite coating for spherical inclusions and the effective quantity depends only on the dielectric functions of the components and their volume fractions. The Maxwell-Garnett theory, in its simplest form, assumes that the medium has a separated grain structure. The Bruggeman and Ping Sheng theories on the other hand, apply to a two-component mixture having aggregate microstructure. The Ping Sheng model derives for the more general case of coated particles in an effective medium. The differences in microstructures between the mentioned theories have indeed an effect on the modelled optical properties of the composite.

Bruggeman's model calculates the Bruggeman effective dielectric function, ε_{Br} , for a composite of two different media, a and b with specific volume fractions i.e. fill factors f_a and f_b =1- f_b with their respective dielectric functions ε_a and ε_b . The model is based on a random mixture of the two components according to Figure 6 (a) and (c).

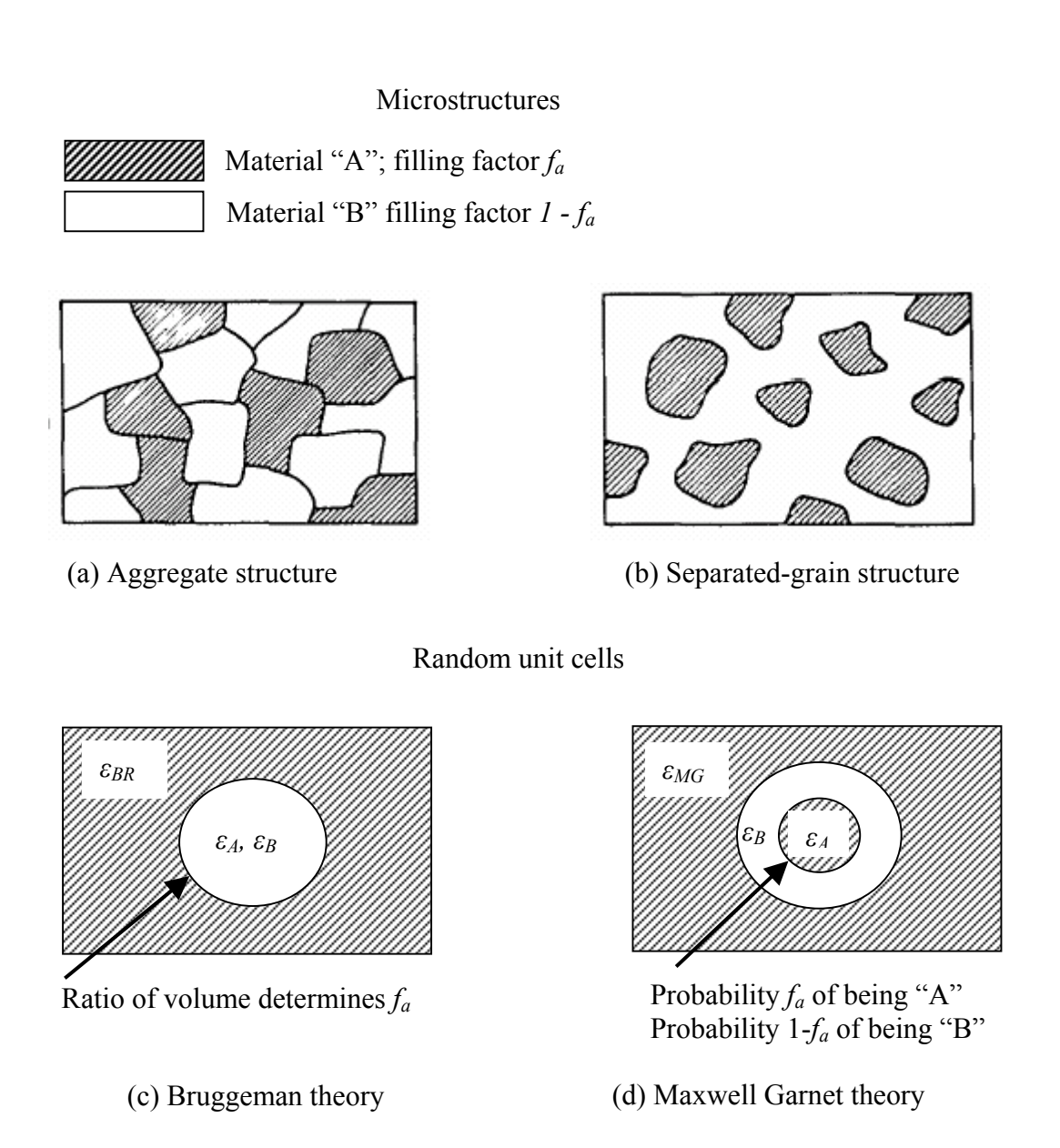


Figure 2.12. Microstructures of (a) aggregate, (b) separated-grain structures for a two component medium, (c) and (d) are random unit cells (RUC) to derive the effective dielectric function of the aggregate (Bruggeman model) and separated grain (Maxwell-Garnett) structures, respectively.

In the case for particles shaped as small spheres, the model is expressed by equation (2.35).

$$f_a \frac{\varepsilon_a - \varepsilon_{Br}}{\varepsilon_a + 2\varepsilon_{Br}} + (1 - f_b) \frac{\varepsilon_b - \varepsilon_{Br}}{\varepsilon_b + 2\varepsilon_{Br}} = 0$$
(2.35)

The Maxwell-Garnet theory corresponds to Figure 2.12(b) and (d) and is given by equation (2.36):

$$\frac{\varepsilon_{MG} - \varepsilon_b}{\varepsilon_{MG} + 2\varepsilon_b} = f_a \frac{\varepsilon_a - \varepsilon_b}{\varepsilon_a + 2\varepsilon_b} \tag{2.36}$$

where ε_{MG} is the Maxwell-Garnet effective dielectric function for a two-component composite. Equation (2.36) can be solved to give:

$$\varepsilon_{MG} = \varepsilon_b \left[\frac{\varepsilon_a + 2\varepsilon_b + 2f_a(\varepsilon_a - \varepsilon_b)}{\varepsilon_a + 2\varepsilon_b - f_a(\varepsilon_a - \varepsilon_b)} \right]$$
(2.37)

There is a basic difference between Maxwell-Garnett and Bruggeman theories. Bruggeman assumes the composite to consist of randomly intermixed particles of dielectric and metal whereas Maxwell-Garnett considers the metal to be dispersed as particles through the dielectric or vice versa. Their dielectric functions are however, similar at low filling factors. Both theories have in common that the effective dielectric function does not depend explicitly on the size of the inhomogeneities.

2.5.4. Absorber materials for high temperatures

For concentrating solar power (CSP) systems applications, the spectrally selective surfaces should be thermally stable above $400~^{0}$ C in air. Many selective surfaces capable of operating at temperatures greater than $400~^{0}$ C have been developed. Ni-pigmented Al₂O₃, graded Ni-NiO, black graded Mo or W-Al₂O₃ and double SS-AlN cermets are commonly available.

By using metals and dielectrics that are stable at higher temperatures and incorporating multiple AR coatings and multiple cermet coatings along with the appropriate texturing, materials could be improved or developed closer to the CSP requirements. Optical modelling of the potential high-temperature selective surfaces should be performed to identify and select the coating thickness and composition of the most promising candidates. The most promising candidates would be made and tested. The capability should be built to allow spectrally selective coatings to be exposed and measured at their operating temperatures and conditions for longer periods of time to determine the durability and thermal stability of the material.

2.6. Optical characterization instruments

2.6.1. The UV/Vis/NIR LISR-3100 spectrophotometer

The optics of the integrating sphere assembly of the Shimadzu LISR-3100 spectrophotometer is shown in Figure 2.13. The diagram the reference light and the sample light already separated.

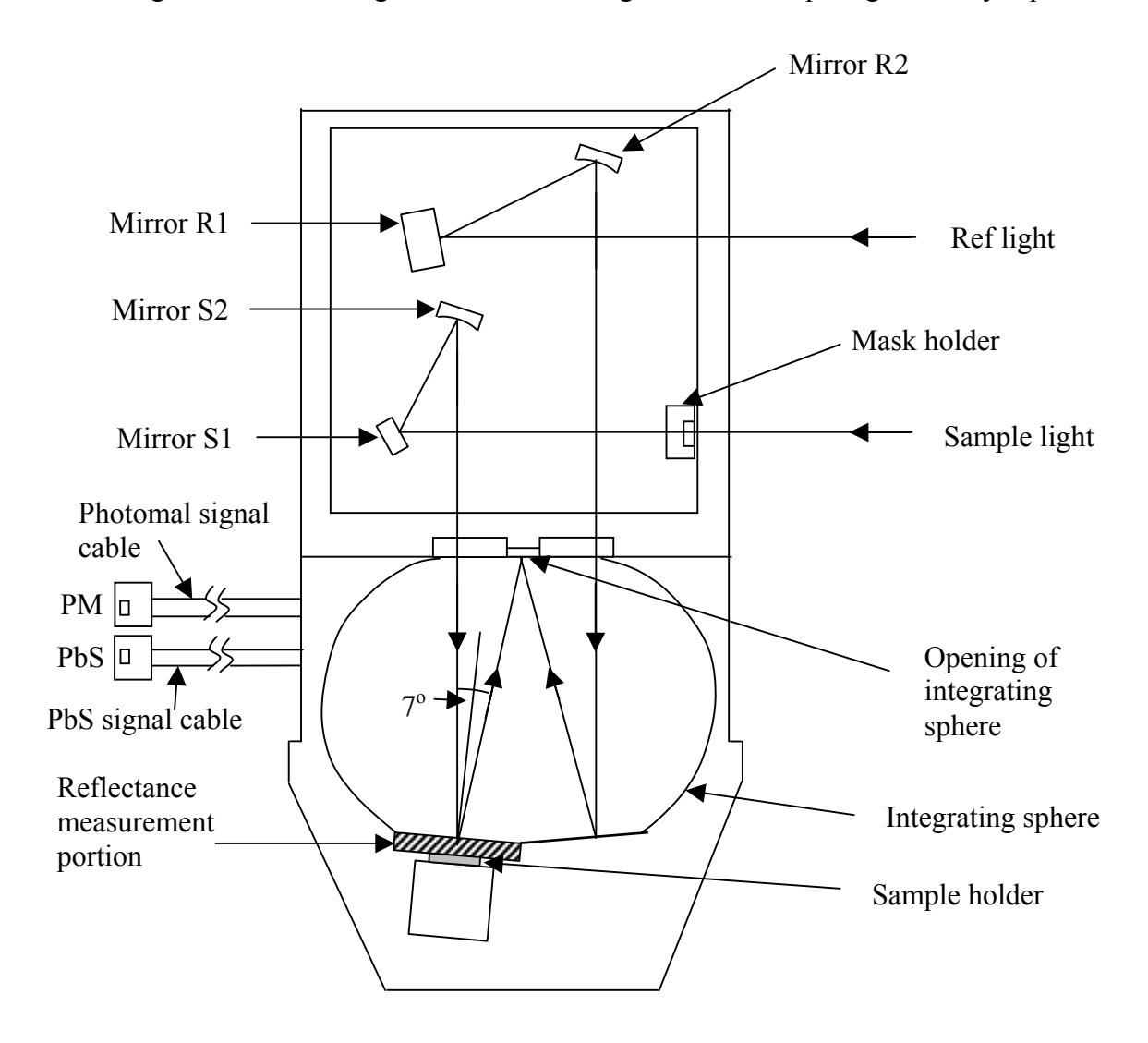


Figure 2.13. The optics of the LISR-3100 spectrophotometer.

Sample light is incident on mirror S1 that reflects it onto mirror S2. The light is then reflected onto the sample, which absorbs some radiation. The remaining radiation is then reflected onto

the opening of the integrating sphere where there is a detector to compare the sample and the reference radiation. Reference light from the source is incident on mirror R1 that reflects it onto Mirror R2 that again reflects the light onto a flat part of the integrating sphere. Here the light is directed towards the detector.

The whole system is interfaced to a computer. The spectra obtained can be printed from the computer.

2.6.2. The M500 IR spectrophotometer

The Buck M500 IR spectrophotometer is a single beam, microprocessed, and ratio recording spectrometer. Its ray diagram is shown in Figure 2.14.

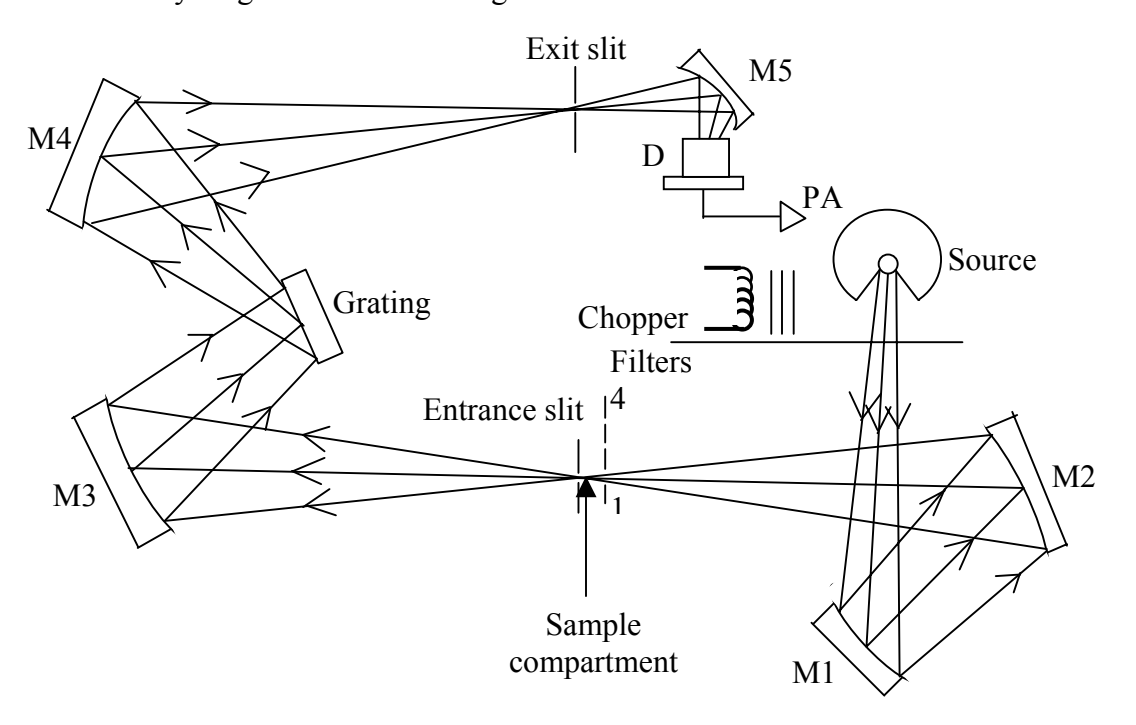


Figure 2.14. The optical diagram of the M500 IR spectrophotometer.

The two mirrors to the right of the sample compartment (M1 and M2) condense and focus the source image through the full-size sample compartment. The sample compartment is designed to accommodate a reflectance accessory Figure 2.15.

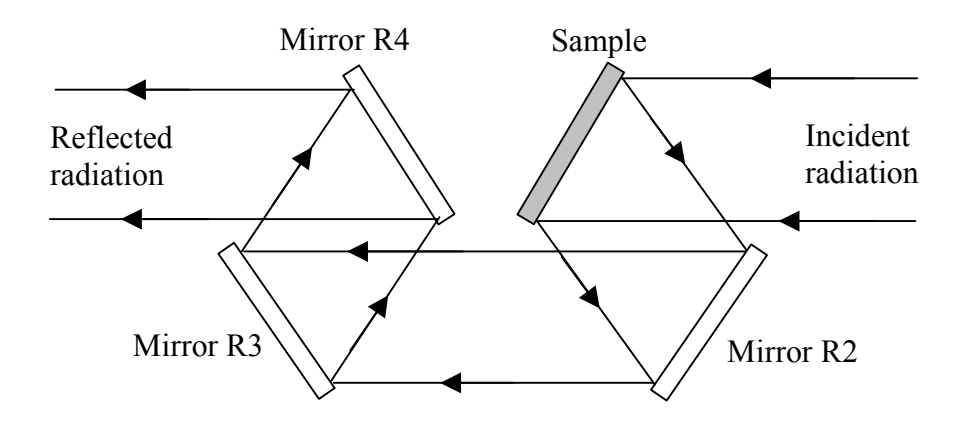


Figure 2.15. The reflectance accessory with a sample fitted in place.

From the sample the light goes through one of the four cut-on filters that keep higher orders of light from entering the monochromator. From the entrance slit, light goes onto the first collimating mirror, (M3), which directs the light onto the grating. The 75 lines per millimetre grating disperse the light and send it to the second collimating mirror (M4). The second collimator focuses the light through the exit slit. Mirror M5 focuses the energy down to a 1mm by 2mm Deuteriated L-Alamine Sulphate (DLATGS) detector, D, on the pre-amp board. The analogue signal is sent to the main system board to be filtered, amplified and microprocessed.

When determining the performance of the solar absorber, the total reflectance is measured in the solar and infrared wavelength ranges, from $0.3 \mu m$ to $50 \mu m$. The measured reflectance can be

used in equations 1 and 2 to calculate the solar absorptance and thermal emittance. The reflectance data are extrapolated from 20 μ m to 100 μ m for calculations of the thermal emittance. This instrument was assembled and tested by Makiwa [40].

CHAPTER 3. EXPERIMENTAL PROCEDURE

3.1. Introduction

The preparation of selective solar absorber coatings using the sol-gel technique requires extreme care. There are a lot of variables that need to be considered starting from the preparation of substrates. It is recommended to alter one variable at any particular time.

Figure 3.1 shows the flow diagram of preparation of selective solar absorber coatings using the sol-gel spin coating process. First the precursor sol has to be prepared and the substrates cleaned. The coating of the substrates using the prepared sol by the spin coating process then follows. The coated substrates are then heat treated after which they can be characterized.

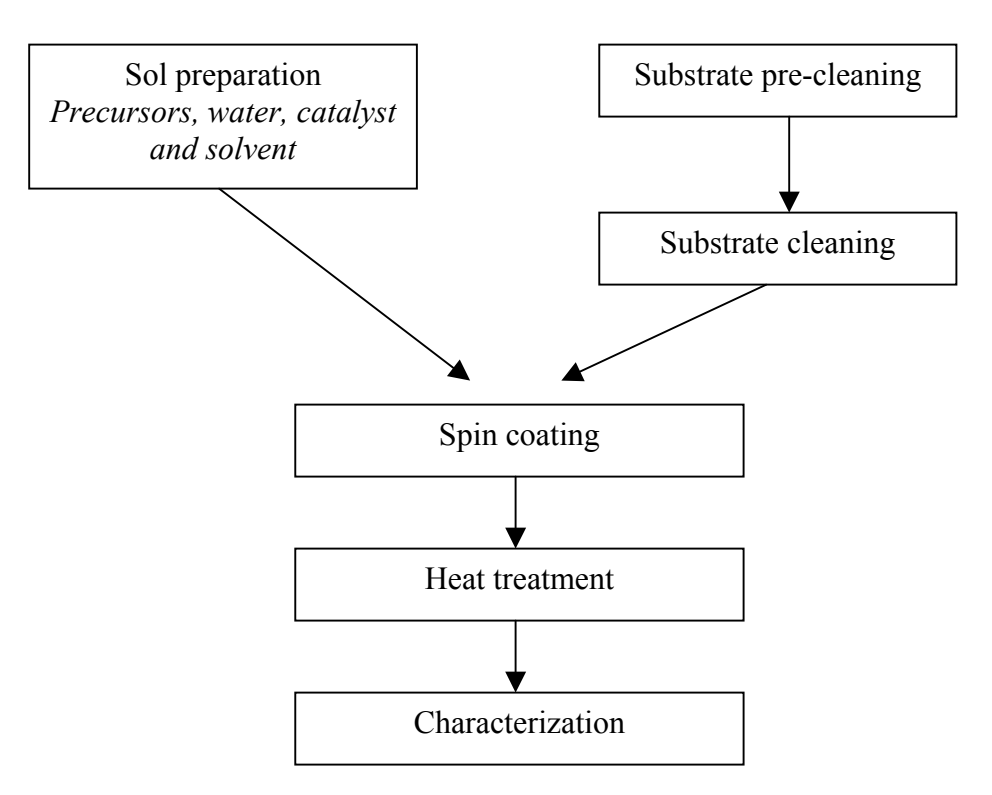


Figure 3.1. Flow diagram of preparation of solar absorber coatings by the sol-gel spin coating process.

3.2. Cleaning of substrates

Two types of substrates namely rough aluminium and stainless steel were used in this research.

These were cut from large sheets. Each of the substrates measured approximately 55 mm by

55 mm. All substrates were pre-washed before being treated in acid baths.

3.2.1. Substrate pre-wash

The substrates were cleaned in mild aqueous detergent first. This served to remove grease particles and some dirt from the substrate surfaces. They were then rinsed thoroughly to remove the detergent and then put in an acid bath.

3.2.2. Removal of oxide layer

Metals like aluminium tend to react with atmospheric oxygen to form a protective oxide layer that must be etched away with an acid.

After the pre-wash aluminium substrates were treated in phosphoric acid ultrasonic bath held at 60 °C for about 45 minutes. The ultrasonic bath makes sure that the substrates are being etched uniformly. Steel substrates were treated in a hydrochloric acid ultrasonic bath held at the same temperature for the same period of time.

After treating the substrates for 45 minutes in the acid baths, they were then rinsed thoroughly in distilled water to remove the acid. To ensure that substrates are clean before drying, a uniform water film must form on the substrates after rinsing in distilled water. The drying of the substrates was carried out by holding the substrates over a hot plate stove. Rapid drying was

avoided since it could cause the water to evaporate fast leaving some dirty on the substrates.

Substrates were only dried a few minutes before the coating to avoid contamination.

3.3. Preparation of C-NiO sol

3.3.1. Chemicals

For the preparation of C-NiO sol, the following materials were used: sucrose (SUC), distilled water, nickel acetate (M=248.84g/mol, (CH₃COO)₂Ni·4H₂O, AR) as precursor, diethanolamine (M=105.14g/mol, NH(CH₂CH₂OH)₂, DEA, AR) as chelating agent, ethanol (M=46.07g/mol, CH₃CH₂OH, EtOH, AR) as solvent and polyethylene glycol (M=2000g/mol, H(OCH₂CH₂)_n, PEG, AR) as organic template.

PEG was manufactured by Sigma Chemical company (USA). Nickel acetate was manufactured by British Drug House LTD (England). DEA was manufactured by Riedel-de Haën AG (Germany). Ethanol was manufactured by Petuna Laboratories (Zimbabwe).

3.3.2. Preparation steps

The preparation of C-NiO sol was done by following the order of steps listed below. 100ml plastic bottles were used as containers throughout this research. The stirring was done using magnetic stirrers.

- 0.03 moles (7.4652 g) of nickel acetate were added to 50 ml of ethanol. The mixture was stirred for 1 hour at room temperature to make sure that all the nickel acetate had dissolved.
- 2. 0.06 moles (6.3084 g) of DEA were added to the solution in 1 above. The solution was stirred for 5 minutes.

- 3. Different amounts of organic template, PEG were added to the solution. Stirring was done for 5 minutes until all PEG had dissolved and there was complete mixing.
- 4. Different concentrations of sucrose (SUC) solution were added to the mixture. Stirring was done for one minute.

At this point the sol was ready for deposition. The SUC starts to react with the sol to produce an emulsion. If this happens before deposition then the sol is no longer useful. It is said to have gone bad. One of the objectives of this research is to vary the SUC concentration to find out the optimum SUC concentration. The above order is very crucial since changing it will result in materials with different optical properties. Also, changing the concentration of any ingredient and the stirring time has the same effect as stated above. Care must be taken to vary only one variable for any investigation. Table 3.1 shows the different carbonization temperatures and relative amounts of CH₃COO)₂Ni·4H₂O, DEA, H₂O, PEG and SUC used in the different sols. A column not filled indicates that the variable was kept constant.

Table 3.1. Heat treatment temperature and chemical compositions used in the preparation of NiO sols.

Temperature	Spin	CH ₃ COO) ₂ Ni·4H ₂ O	DEA (g)	PEG (g)	H ₂ O (g)	SUC (g)
(°C)	coating	(g)				
	speed					
	(rpm)					
550	3000	6.585	6.3084	1.0	6.0	6.0
550	3000	6.585	6.3084	1.0	6.0	7.0
550	3000	6.585	6.3084	1.0	6.0	8.0
550	3000	6.585	6.3084	1.0	6.0	9.0
550	3000	6.585	6.3084	1.0	6.0	10.0
550	3000	6.585	6.3084	1.0	6.0	11.0
550	3000	6.585	6.3084	1.0	6.0	12.0
550	3000	6.585	6.3084	0.5	6.0	8.0
550	3000	6.585	6.3084	0.7	6.0	8.0
550	3000	6.585	6.3084	1.0	6.0	8.0
550	3000	6.585	6.3084	1.5	6.0	8.0
550	3000	6.585	6.3084	2.0	6.0	8.0
550	2000	6.585	6.3084	1.0	6.0	8.0
550	2500	6.585	6.3084	1.0	6.0	8.0
550	3000	6.585	6.3084	1.0	6.0	8.0
550	3500	6.585	6.3084	1.0	6.0	8.0
550	4000	6.585	6.3084	1.0	6.0	8.0
550	4500	6.585	6.3084	1.0	6.0	8.0
550	5000	6.585	6.3084	1.0	6.0	8.0
300	3000	6.585	6.3084	1.0	6.0	8.0
350	3000	6.585	6.3084	1.0	6.0	8.0
400	3000	6.585	6.3084	1.0	6.0	8.0
450	3000	6.585	6.3084	1.0	6.0	8.0
500	3000	6.585	6.3084	1.0	6.0	8.0
550	3000	6.585	6.3084	1.0	6.0	8.0

Aluminium substrates were used for all these experiments. Steel substrates were only used when the effects of temperature were being investigated. The effect of heating steel substrates was also investigated by heating them in air at temperatures of 300 °C to 800 °C for 1 hour.

3.4. Preparation of C-SiO₂ sol and the chemicals used

3.4.1. Chemicals

For the preparation of C-SiO₂ sol the following materials were used: distilled water, SUC, hydrochloric acid (HCl), tetraethyl orthosilicate (M=208.33 g/mole, (C₂H₅O)₄Si, TEOS, AR) and methyl trimethoxysilane (M=178.3, Si(OCH₂CH₃)₃CH₃, MTES, AR).

HCl was manufactured by Petuna Laboratories (Zimbabwe). TEOS and MTES were manufactured by Sigma-Aldrich (Germany).

3.4.2. Preparation steps

The preparation of C-SiO₂ sol was done by following the order of steps listed below:

- 1. 100 ml of distilled water were put into a plastic bottle. Drops of HCl were added until the pH was 2. While drops of HCl were being added the water was stirred continuously to make it homogeneous. Measurements of pH were done using universal indicator paper made by Macherey-Nagel GmbH & Co (Germany).
- 2. 6 g of SUC were added to 9 g of the acidified water prepared in step 1. Stirring was done until all the SUC had dissolved.
- 3. 12 g of TEOS were added to the solution. The solution was stirred for 5 minutes in order to make a homogeneous sol.
- 4. 2.4 g of MTES were added to the solution. This time the stirring was done for 12 hours. Stirring for along period of time results in a homogeneous mixture.

After step 4, the sol was ready for deposition. Table 3.2 shows the temperature and chemical compositions used in the preparation of SiO₂ sols. Temperature was the only variable investigated here. All the other variables were kept constant.

Table 3.2. Heat treatment temperature and chemical compositions used in the preparation of SiO_2 sols.

Temperature (°C)	TEOS (g)	MTES (g)	$H_2O(g)$	SUC (g)
300	12.0	2.4	9.0	6.0
350	12.0	2.4	9.0	6.0
400	12.0	2.4	9.0	6.0
450	12.0	2.4	9.0	6.0
500	12.0	2.4	9.0	6.0
550	12.0	2.4	9.0	6.0

3.5. Synthesis

The coating was done using a P-6708D 8" desktop precision spin coating system. This spin coater was programmed in such a way that it could rotate at the coating speed for 20 minutes as shown in Figure 3.2.

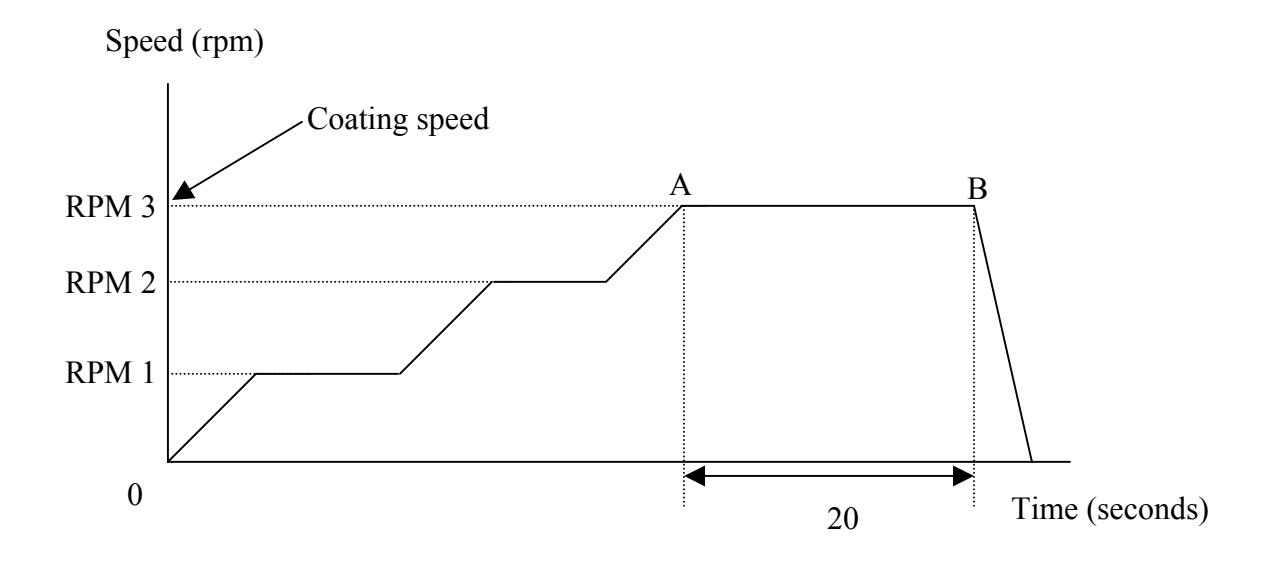


Figure 3.2. The non-dispensing cycle of the P-6708D spin coater.

The dispensing with this instrument is done manually using a syringe and was done at point A on the figure. For all coatings made, the amount of sol dispensed onto the rotating substrate was 2 ml. This was done to avoid differences in the thicknesses of the coatings. Increasing the amount of sol added to the rotating substrate has the effect of increasing the thickness of the thin films formed. After the coating the samples were put into a tube furnace for carbonization.

3.6. Heat-treatment of samples

The heat-treatment (carbonization) was done using a tube furnace manufactured by Enteck Ängelholm Company (Sweden). The samples were pushed into the tube of the furnace in which nitrogen gas was continuously being pumped in to produce an inert atmosphere. The furnace temperature was raised to the desired temperature, T_M at 5 °C min⁻¹, maintained at that temperature for 60 minutes and then cooled to 25 °C at 20 °C min⁻¹ (Figure 3.3). Samples were ready for characterisation thereafter.

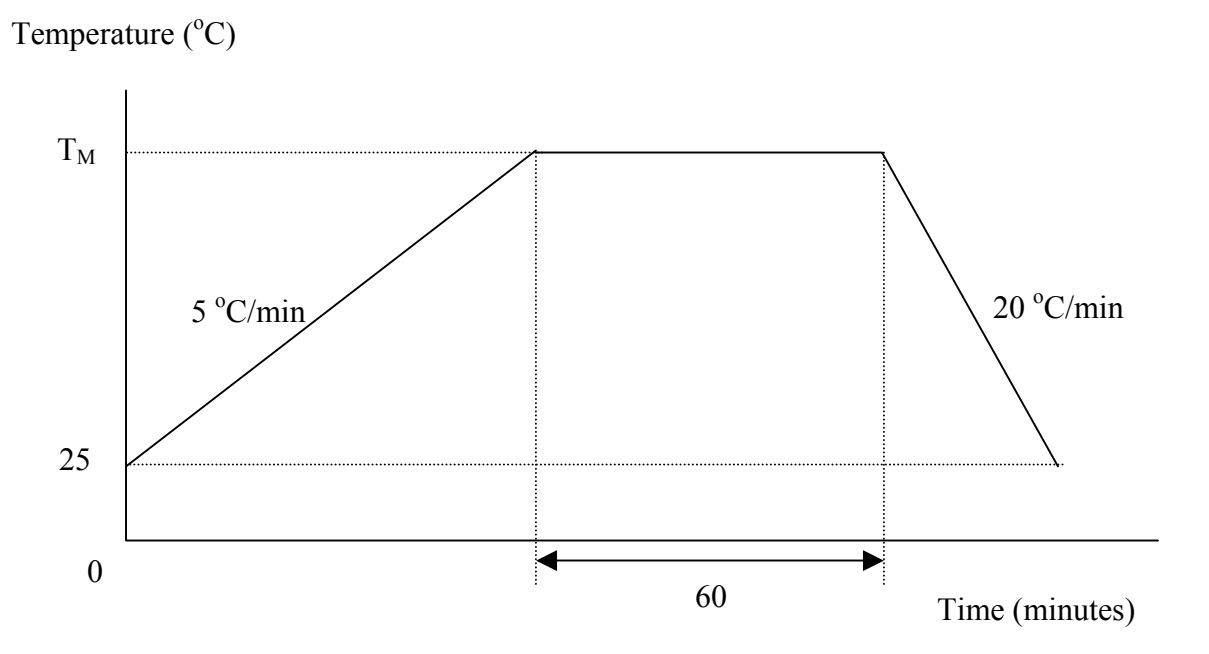


Figure 3.3. The heat-treatment process.

3.7. Optical characterization

3.7.1. UV/Vis/NIR measurements

The Shimadzu LISR-3100 UV/Vis/NIR spectrophotometer from the chemistry department was available for the solar spectrum range. A brief description of the most important parts of the instrument is given in Section 2.7.1. The angle of incidence of the sample beam is 7°. A BaSO₄ standard white plate was put at the reflection measurement portion and a baseline correction was made. In order to obtain spectra for the samples the standard white plate was replaced with the samples. Scans were run at different positions of the samples to see if the spectra were repeatable.

3.7.2. IR measurements

The IR measurements were done using the Buck M500 IR spectrophotometer described in Section 2.7.2. This instrument does not have an integrating sphere. The reflectance accessory (Figure 3.5) has an angle of incidence of. The baseline correction was done with a mirror in the sample position. The mirror was then replaced with a sample to obtain a sample scan. The scan was converted to a percentage reflectance spectrum. The data points were copied and combined with that obtained with the Shimadzu LISR-3100 spectrophotometer using Excel. The plotting of the spectra was redone using Kaleidagraph and Matlab programs. Calculation of absorptance and emittance were done using a Matlab program that incorporates equations (2.20) and (2.21). The limits were $\lambda_1 = 0.3 \ \mu m$ and $\lambda_2 = 2.5 \ \mu m$ for the solar absorptance and $\lambda_1 = 2.5 \ \mu m$ and $\lambda_2 = 100 \ \mu m$ for the thermal emittance.

CHAPTER 4. RESULTS AND DISCUSSION

4.1. Introduction

The results of the experiments described in Chapter 3 are presented here in parts. Each part relates to one type of experiment and also includes a discussion of the results. Reference is made often to experimental results from other spectrally selective solar absorber systems. An analysis of the IR spectra obtained with the M500 IR spectrophotometer will now be presented.

4.2. IR reflectance measurements

The reference spectrum obtained after running a reference scan is shown in Figure 4.1. The spectrum shows that the reflectance is about 32 % at a wavenumber of 4000 cm⁻¹. A similar scan done for the straight through position in air gave a transmittance of 56 % at the same wavenumber. Water absorption bands are shown at wavelength ranges of about 3650–3850 cm⁻¹ and 1350 - 1900 cm⁻¹. Absorption bands for CO₂ are shown at wavelengths of approximately 2470 cm⁻¹ and 680 cm⁻¹. Also included in the spectra are the instrument effects of the grating and filter change. The effect of the grating anomaly is shown at a wavelength of approximately 850 cm⁻¹ and that of filter change is shown at wavelengths of about 1000 cm⁻¹, 1980cm⁻¹ and 3050 cm⁻¹. The reflectance spectrum was obtained by running two scans, one for the reference mirror and another for the sample. This process cancels out the grating anomaly and the filter change effects.

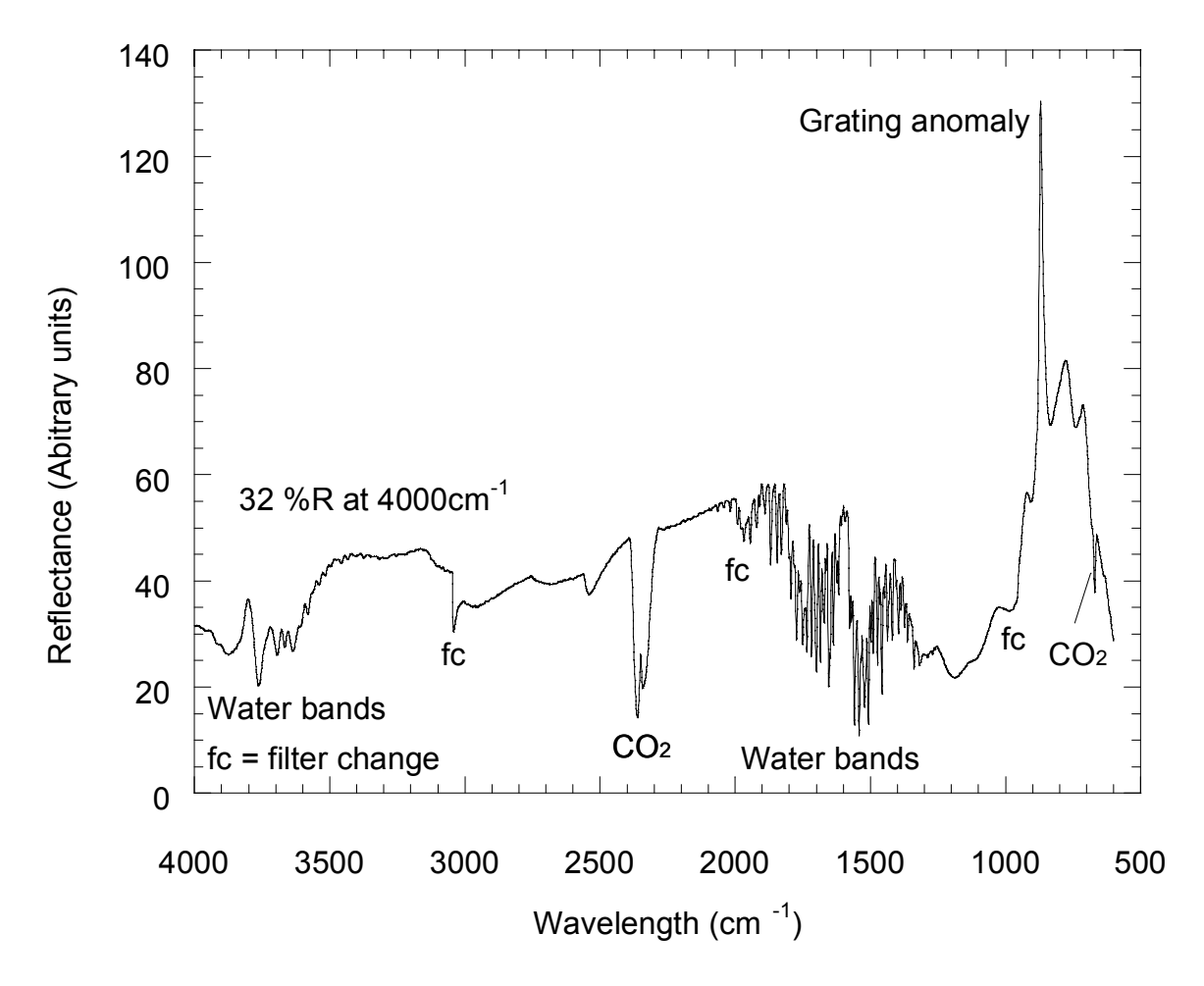


Figure 4.1. Reflectance spectrum obtained when the reference mirror was in the sample position.

4.3. Analysis of C – NiO composite films.

The hemispherical reflectance spectra for samples used for the different investigations in this work are shown in Figures 4.2 to 4.8.

Figure 4.2 shows the spectral reflectance of a sample of NiO/Al without sucrose (SUC). The pattern shown in the graph is similar to the one shown for black nickel by Zerlaut [60] and the oscillations shown in the UV/Vis/NIR are typical of black nickel.

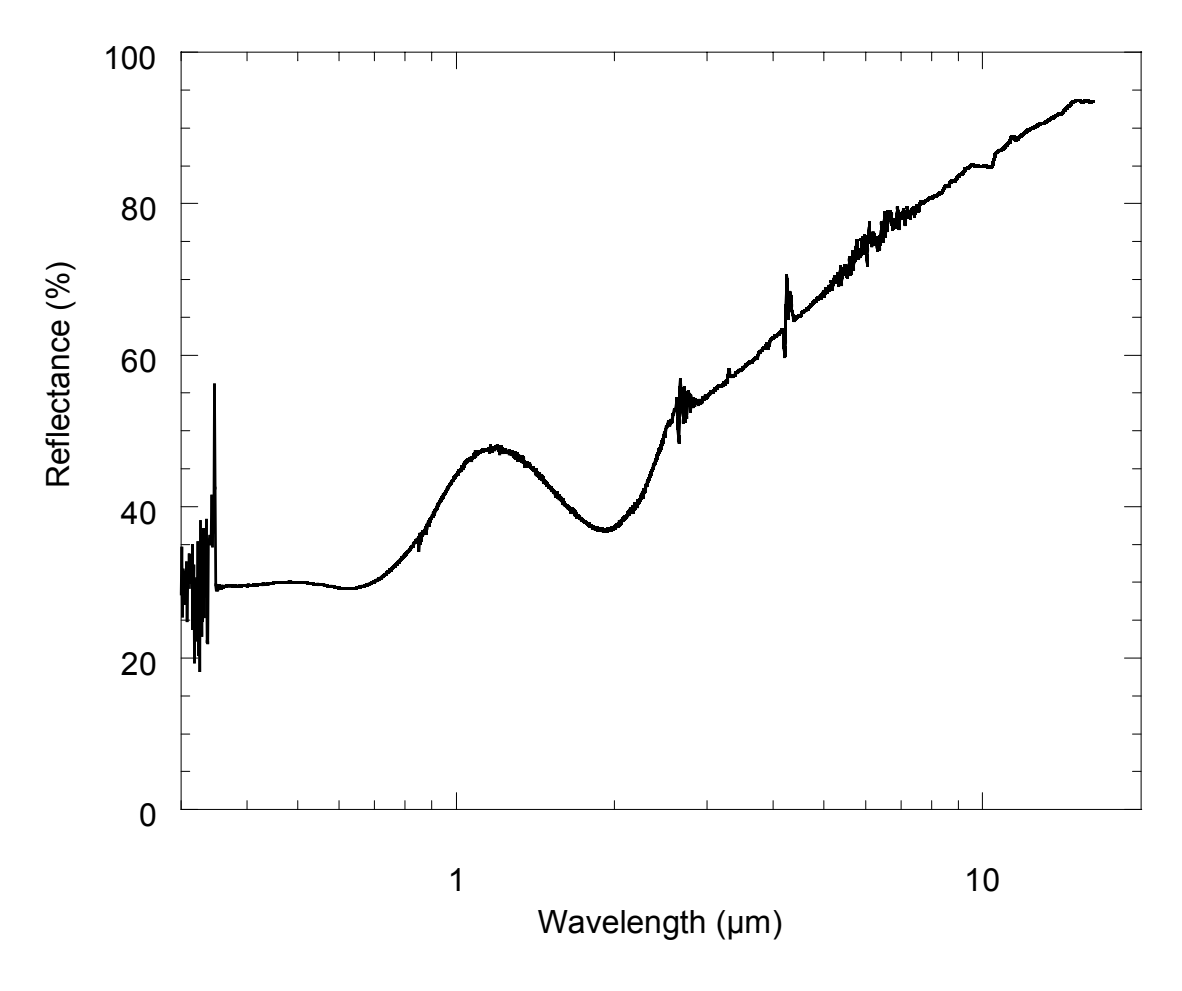


Figure 4.2. Spectral reflectance of a NiO sample without SUC

The reflectance of the sample increases from around 30 % at 0.35 μ m to about 95% at 16 μ m. The crossover occurs at about 2.5 μ m. The reflectance in the UV/Vis/NIR range starts with a lot of noise. This is due to the design of the instrument. It stabilises at a wavelength of about 0.35 μ m. For this reason, all the spectra will be considered to be starting at 0.35 μ m.

The graph shows that at a wavelength of $0.35~\mu m$ the reflectance is about 30 %. It stays at this value up to a wavelength of 7 μm from which interference effects manifest. The positions of maxima and minima in the interference depend on the film thickness. From 2 μm onwards it keeps on increasing. It ends at about 95% when the wavelength is $16~\mu m$. The discontinuity in

the gradient of the graph at $2.5~\mu m$ is due to the differences in the two instruments used to make measurements in the UV/Vis/NIR and in the IR wavelength ranges.

The calculated values for the absorptance and emittance are 0.70 and 0.27 respectively. All absorptance and emittance values calculated in this report were done using a Matlab program provided by Katumba *et al.* [7] and confirmed by a formula given by Duffie [15].

4.3.1. Effect of amount of carbon precursor (SUC) on C-NiO/Al samples

Figure 4.3 shows the effect of adding SUC on the NiO. The shape of the spectra shows that two regions exist. As expected, the reflectance in the solar spectral range (0.3 to 2.5 μ m) is below 50 % and that in the IR is above 50 % for a greater number of the samples. In the solar spectral

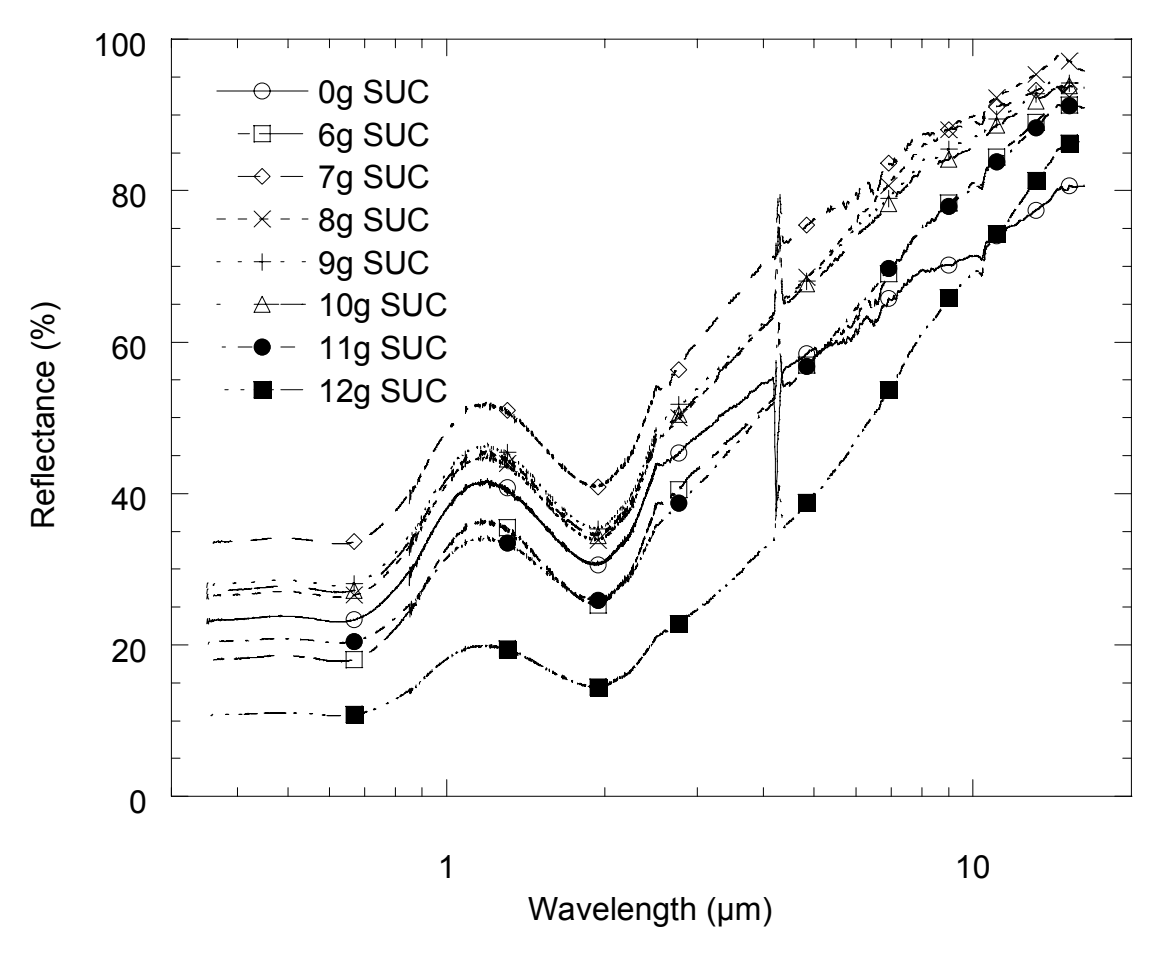


Fig 4.3. Effect of amount of SUC on C-NiO/Al samples.

range, the pattern for the spectra is the same. Samples with 12 g SUC have the least reflectance and samples with 7 g SUC have the highest reflectance. It is expected that the sample with 0 g SUC would have the highest reflectance. There are two probable reasons why some samples with SUC have a higher reflectance than that without. The first and most probable reason is the differences in the instruments used as implied by the gradients of the two sections of the graph for the 0 g SUC sample. The second reason could be that the chemical changes that took place when the samples were being heated were different for the samples with different amounts of SUC.

In the IR range, the reflectance increases at constant rate for all samples except for that of the sample without SUC. The reflectance for the sample without SUC increases at a slower rate than that for samples with SUC. This is evidence that SUC increases the absorptance in the solar spectral range.

Addition of 6 g SUC results in samples with a higher reflectance in the solar spectral range and a higher reflectance in the IR range. A suggested cause for this is the reduction of NiO by carbon during carbonization. This reduction process produces Ni on the substrates and carbon dioxide gas. This means that the amounts of NiO and carbon on the substrate are being reduced. A way of slowing down this reduction reaction is needed to solve this problem. The work reported here did not involve finding a solution to this. The spectra show that even if this reaction is taking place the reflectance of what remains on the substrate is not affected much. The reason for this is that a composite of Ni and NiO over aluminium substrates is also a good solar absorber [3]. A report given by Kennedy [3] shows that the Ni-NiOx composite thin films investigated were

fabricated using reactive sputtering. Tabor [54] has also described black nickel as a selective solar absorber.

Samples with SUC contents from 7 to 11g show a decrease in reflectance with increasing SUC content in the solar spectral range. Samples with 12 g SUC gave the least reflectance in both regions. A suggested explanation for this behaviour is the increase of carbon content on the absorbing surface. More carbon results in an increase in absorption. It is also observed that as the SUC composition increases from 6 g, the crossover shifts to the IR range. In the IR region the reflectance of the samples with low SUC content is higher than that of samples of higher SUC content. This behaviour was also noticed by Katumba *et al.* [7]. The suggested explanation is that samples of low SUC content are thinner that those of higher SUC content spin coated at the same speed. An increase in SUC content increases the viscosity of the sols. Sols that are more viscous give thicker films because they do not spread easily. An optimum SUC content had to be sought.

Table 4.1 shows the calculated values for α_{sol} , ϵ_{therm} and $\alpha_{sol}/\epsilon_{therm}$. The optimization was done by choosing the samples with the highest $\alpha_{sol}/\epsilon_{therm}$ ratio. From this Table it is clear that the ratio increases with SUC content up to 8 g SUC and then starts to decrease with the continued addition of SUC. The optimum SUC content for samples with high absorptance and low emittance was chosen to be 8 g SUC. These samples had an added advantage in that they stayed for a considerable amount of time without turning into a suspension (Table 4.1).

Table 4.1. The dependence of the ratio of solar absorptance to thermal emittance of C-NiO/Al samples with SUC content.

Amount of SUC	Time taken	Solar absorptance,	Thermal	α_{sol} / ϵ_{therm}
(g)	before sols	$lpha_{ m sol}$	emittance, ε_{therm}	
	went bad (hrs)			
0	48.00	0.7017	0.2726	2.5741
6	1.00	0.7540	0.1940	3.8866
7	0.75	0.5988	0.1136	5.2711
8	0.50	0.6694	0.1119	5.9821
9	0.25	0.6542	0.1318	4.9636
10	0.17	0.6627	0.1408	4.7067
11	0.08	0.7465	0.1951	3.8262
12	0.05	0.8594	0.2948	2.9152

4.3.2. Effect of amount of PEG on C-NiO/Al samples

Figure 4.4 shows the effect of PEG on C-NiO/Al samples. The reflectance spectra of the samples studied are much spread in the solar spectral range and they seem to merge in the IR range. It can be seen that samples without PEG have lower reflectance in the solar spectral range. The reflectance of samples increases as PEG is added and is maximum at 1.0 g PEG. It then starts to decrease as th amount of PEG is increased further. In the IR range the reflectance for the sample without PEG rises faster than that for other samples. This is evidence that PEG lowers the absorptance of the samples. It has little effect in the IR region. Samples with 1.0 g PEG have the highest reflectance in both regions.

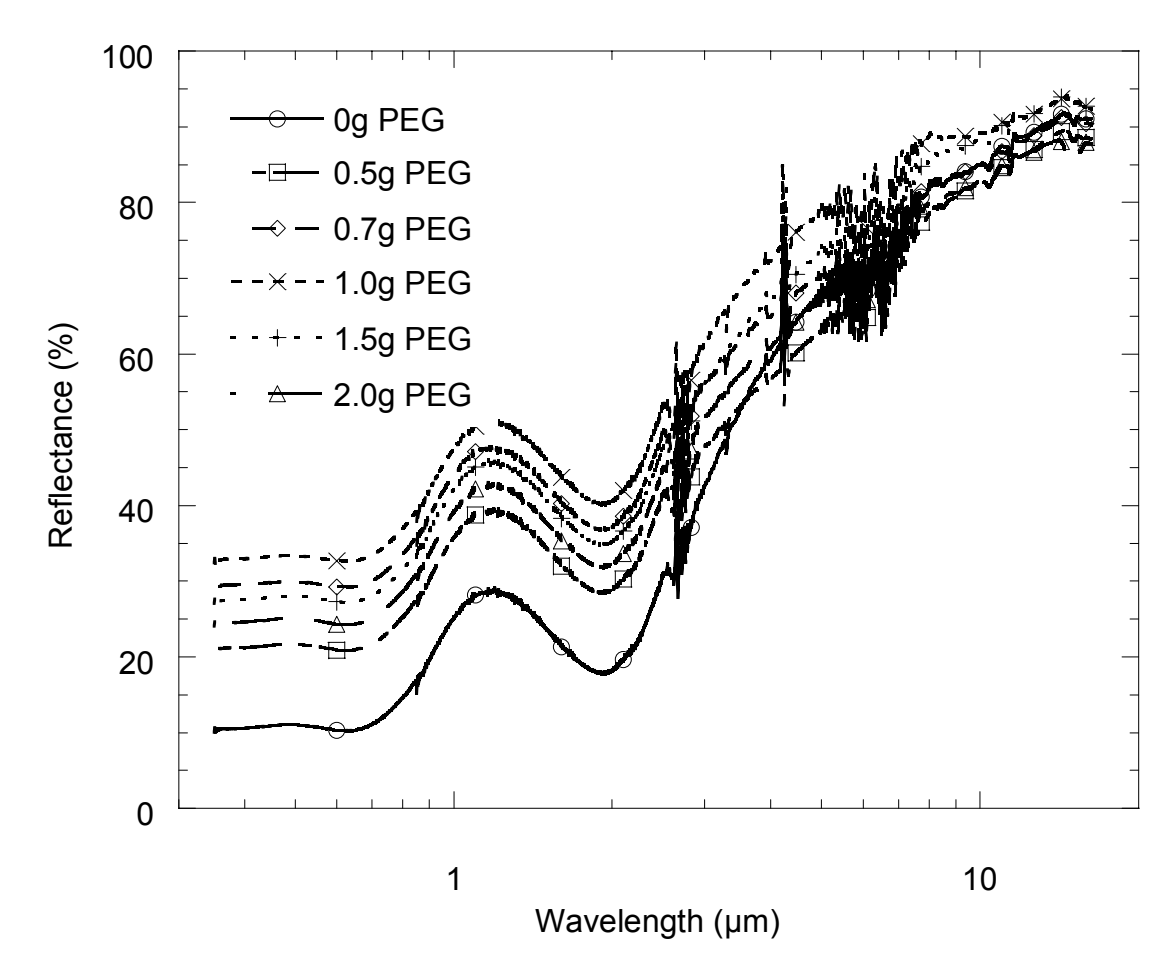


Figure 4.4. Effect of amount of PEG on C-NiO/Al samples.

From the results one would choose not to use PEG in the preparation of samples. Zhifeng *et al.*[25] has shown that the morphology of ZnO thin films depended much on PEG content. Their results show that films without PEG are compact; they become porous with appropriate PEG amount. The porosity disappears gradually with further increase of PEG content. The results obtained in this investigation show that compact films (no PEG) have lower reflectance hence higher absorptance than porous films. This is supported by the calculated values in Table 4.2, which shows that samples without PEG have the highest α_{sol} / ϵ_{therm} ratio. Among the samples with PEG, the ratio is also higher for samples with 1.0 and 1.5 g PEG. The thermal emittance of

the samples with 1.0 g PEG is lower than that for other samples. The optimum PEG content was chosen as 1.0 g. The requirement now was to increase the absorptance in the solar spectral range.

Table 4.2. The dependence of the ratio of solar absorptance to thermal emittance for C-NiO/Al samples with PEG content.

PEG (g)	Absorptance, α_{sol}	Thermal emittance,	$\alpha_{sol}/\ \epsilon_{therm}$
		$oldsymbol{arepsilon}_{ ext{therm}}$	
0.0	0.8297	0.1642	5.0530
0.5	0.7235	0.1923	3.7624
0.7	0.6405	0.1618	3.9586
1.0	0.6063	0.1231	4.9253
1.5	0.6599	0.1336	4.9394
2.0	0.6896	0.1876	3.6759

4.3.3. Effect of speed of spin coating on C-NiO/Al samples

Figure 4.5 shows the effect of speed of spin coating on C-NiO/Al samples. For wavelengths less than 2.5 μ m, the reflectance decreased with spin coating speed. This is in disagreement with theory which suggests that the higher the spin coating speed the thinner the film (Section 2.4.4.) and hence the lower the absorptance.

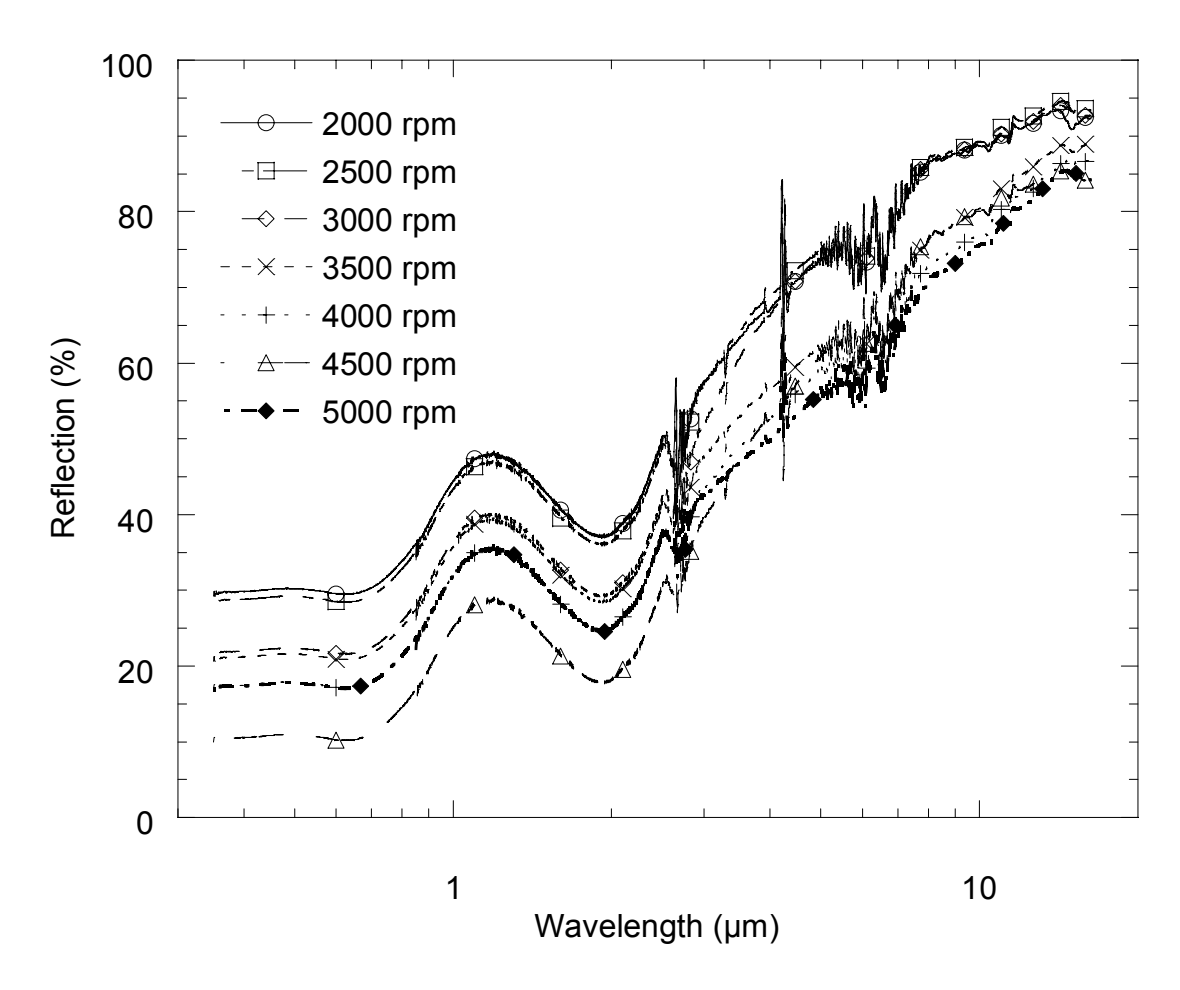


Figure 4.5. Effect of speed of spin coating on C-NiO/Al samples

A possible explanation for this could be that the reduction reaction mentioned in Section 4.3.1 was slowed down probably due to the reduced amount of NiO. This results in less or no carbon being involved in the reduction reaction. More carbon on the absorbing surface increases its absorptance. The higher reflectance of samples spin coated at lower speeds is an indication that there is more NiO on the samples.

An optimum speed was obtained by calculating the α_{sol} / ϵ_{therm} ratio (Table 4.3). The speed that had the highest α_{sol} / ϵ_{therm} value was considered to be the optimum and a value of 3000 rpm was identified and used for the rest of the experiments.

Table 4.3. The dependence of the ratio of solar absorptance to thermal emittance for C-NiO/Al with spin coating speed.

		$lpha_{sol}/$ ϵ_{therm}
	$\epsilon_{ m therm}$	
0.6374	0.1336	4.7710
0.6477	0.1244	5.2066
0.7161	0.1295	5.5297
0.7238	0.2036	3.5550
0.7613	0.2317	3.2857
0.8302	0.2241	3.7046
0.7619	0.2518	3.0258
	0.6477 0.7161 0.7238 0.7613 0.8302	0.6374 0.1336 0.6477 0.1244 0.7161 0.1295 0.7238 0.2036 0.7613 0.2317 0.8302 0.2241

4.3.4. Effect of heat-treatment temperature on C-NiO/Al samples

Figure 4.6 shows the variation of reflection with heat treatment temperature of C-NiO samples. Samples heat-treated at 300 °C and 350 °C have the lowest reflectance in the region of lower wavelengths up to about 8 μm. There is a large increase in reflectance for samples heated at 400 °C. Samples heat-treated at this temperature have the highest reflectance. The reflectance decreases slightly as the temperature is increased beyond 400 °C. The reflectance for all the samples heat-treated at different temperatures merge at higher wavelengths. This is an expected behaviour since the carbonization temperature only affects the carbon content in the samples.

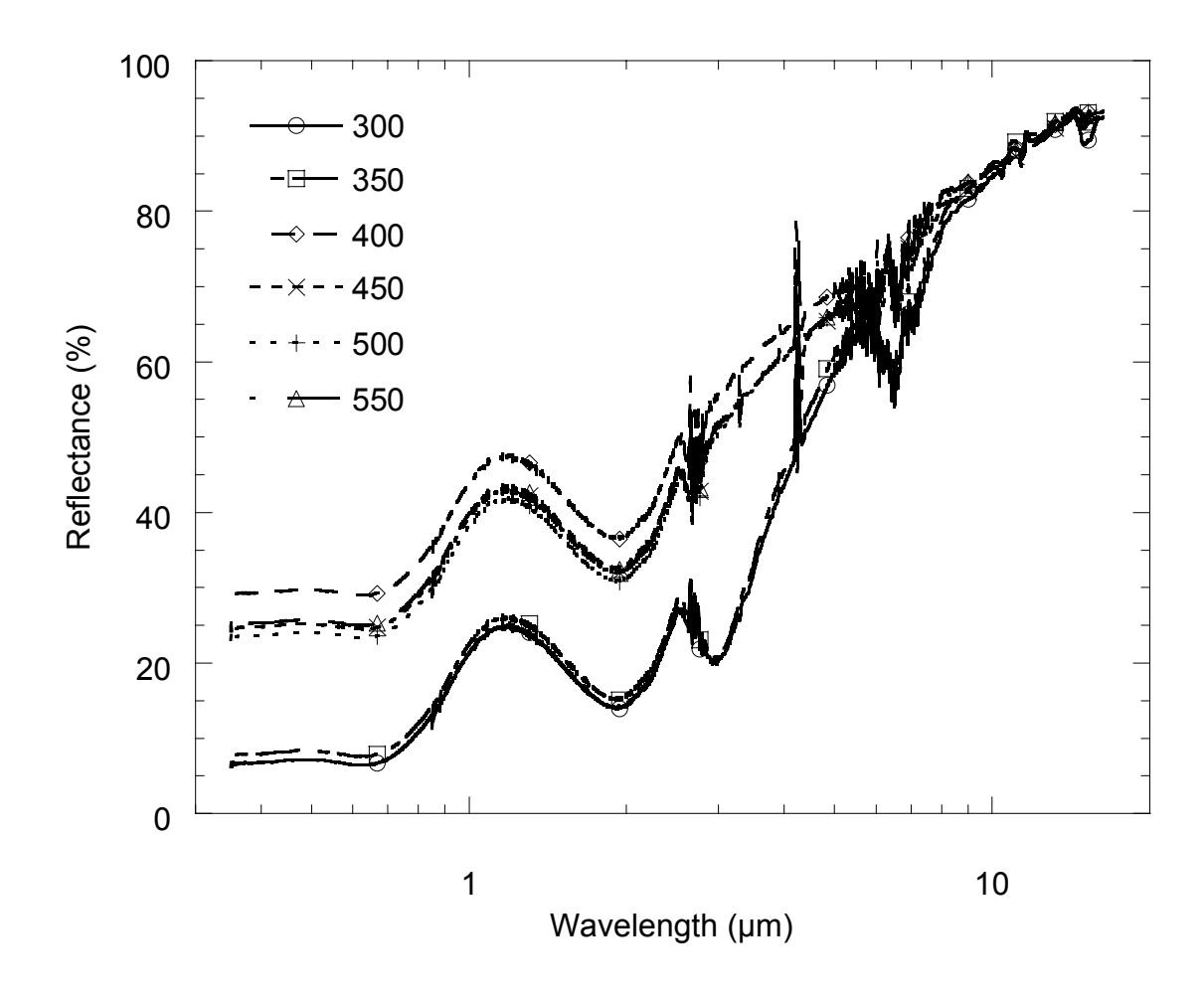


Figure 4.6. Effect of heat-treatment temperature on C-NiO/Al samples.

An explanation for this may be that at lower temperatures, there is more carbon hence the highest absorptance. It is probable that as the temperature is raised, the carbon starts to react with NiO resulting in low absorptance. The small decrease in the reflectance at higher temperatures indicates that the reflectance does not depend much on the heat treatment temperature. At 300 °C the carbonization will already have started since absorptance starts with a higher value.

There is a different trend that appears for the reflectance of samples heat-treated at lower temperatures. An absorption band of one of the carbon bonds appears at about 3 μ m. This confirms that some of the carbon is still linked to other atoms as it will be in organic compounds. The results of the $\alpha_{sol/}$ ϵ_{therm} calculations are presented in Table 4.4. The temperature that had the highest $\alpha_{sol/}$ ϵ_{therm} ratio was 350 °C. This is the temperature at which there is the highest number of carbon atoms in the samples before the number starts to decrease again due to the reduction reaction.

Table 4.4. The dependence of the ratio of solar absorptance to thermal emittance of C-NiO/Al with heat treatment temperature.

Temperature (°C)	Absorptance, α_{sol}	Thermal emittance,	$\alpha_{sol}/\ \epsilon_{therm}$
		$arepsilon_{ ext{therm}}$	
300	0.8682	0.3699	2.3471
350	0.8564	0.3591	2.3849
400	0.6425	0.3380	1.9009
450	0.6879	0.3492	1.9699
500	0.6992	0.3426	2.0409
550	0.6828	0.3426	1.9930

4.3.5. Effect of heat-treatment temperature on NiO/steel samples.

Figure 4.7 shows the variation of reflectance with the carbonization temperature of C-NiO/steel samples. The spectra for samples heat-treated at 300 °C show a similar trend noted for C-NiO/Al

samples in Section 4.3.4. There is an absorption band at 3 μm. This was also noted for the samples heat-treated at the same temperature in Section 4.3.4. As the heat treatment temperature is increased to 350 °C, the absorptance band disappears but the reflectance increases. It is maximum for samples heat treated at 350 °C. Increasing the heat treatment temperature reduces the reflectance. The reason for this is the same as that mentioned for the samples on Al substrates. Samples heat-treated at 400 °C, 450 °C and 500 °C show nearly the same optical properties.

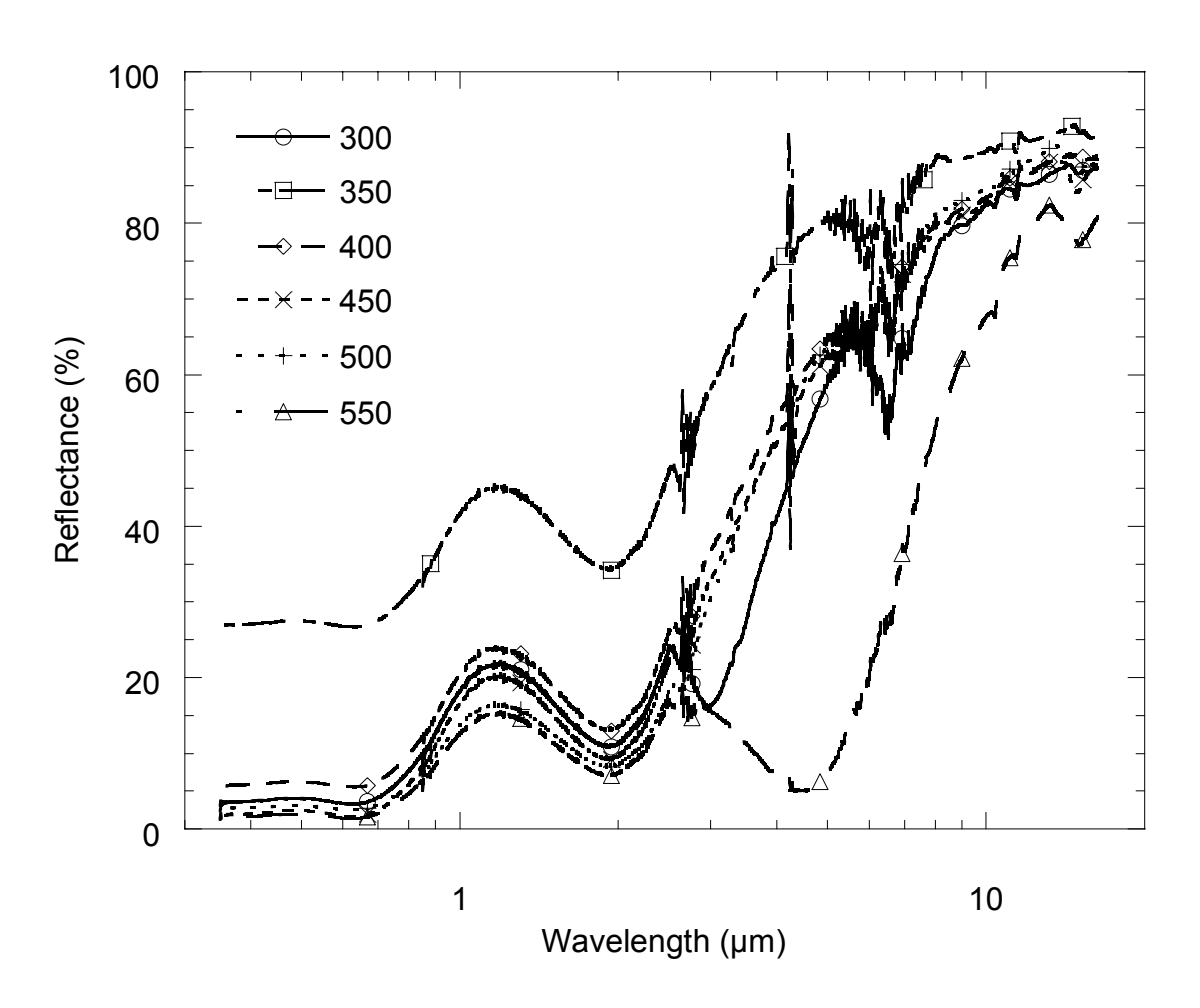


Figure 4.7. Effect of heat-treatment temperature on C-NiO/steel samples.

Deviation from the normal behaviour again occurs at 550 °C. The absorption band that appears for the 300 °C temperature appears again but shifted towards longer wavelengths. This may be due to the change in behaviour of the steel substrates as they are heated. They become dark.

There is an absorption band between 6 and 7 μ m for all samples. This is attributed to the absorption of water by the samples after they have cooled. It could also be absorption from either a carbon-carbon double bond or a carbon-nitrogen double bond.

Table 4.5 shows the calculated values of α_{sol} / ϵ_{therm} for C-NiO/steel samples. The maximum occurs at 350 °C, the same temperature it occurred at for the samples on aluminium substrates.

Table 4.5. The dependence of the ratio of solar absorptance to thermal emittance of C-NiO/steel with heat-treatment temperature.

Temperature (°C)	Absorptance, α_{sol}	Thermal emittance,	$lpha_{sol}/$ ϵ_{therm}
		$arepsilon_{ ext{therm}}$	
300	0.8992	0.2171	4.1419
350	0.6651	0.1229	5.4117
400	0.8773	0.1853	4.7345
450	0.9157	0.1931	4.7421
500	0.9237	0.1780	5.1893
550	0.9350	0.3852	2.4273

4.3.6. Effect of heating steel substrates in air.

Figure 4.8 shows the variation of the reflectance of steel substrates as they are heated. This variation affects the reflectance of coatings done on steel substrates.

It is evident that the reflectance of the steel substrates decreases with temperature. This is confirmed by the fact that the colour of the steel substrates darkens as they are heated. Heating the steel substrates at higher temperatures alters their properties. At 800 °C the steel substrates are nearly black and the absorptance is high. However, the emittance decreases appreciably.

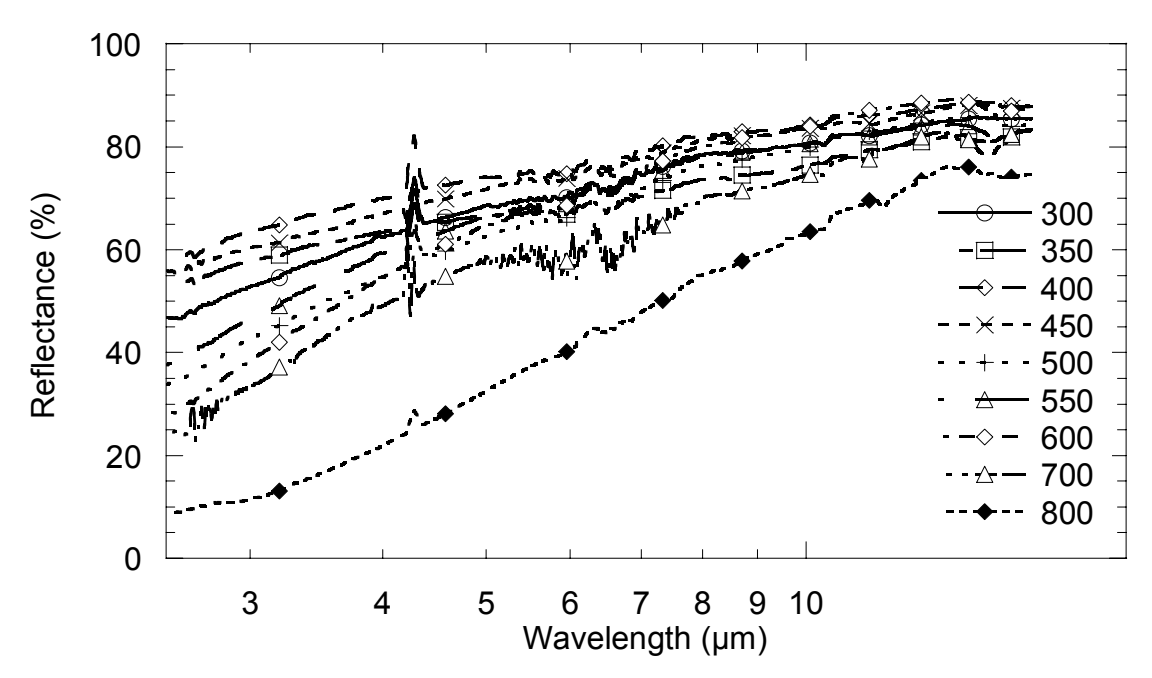


Figure 4.8. Effect of heating steel substrates in air.

4.4. $C - SiO_2$ composite films

C-SiO₂ composite films were fabricated as described in Chapter 3. Figure 4.9 shows the spectral reflectance of a C-SiO₂ sample.

Three major absorption bands can be seen. The absorption band at approximately 9.0 μ m is assigned to stretching vibrations of Si-O-Si or Si-O-X, where X represents ethoxy groups bonded to silicon [7]. The broad absorption band situated at about 3 μ m and one at around 6 μ m are assigned to O-H stretching and O-H bending vibrations, respectively. This is typical of all C-SiO₂ reflectance spectra analysed in this research.

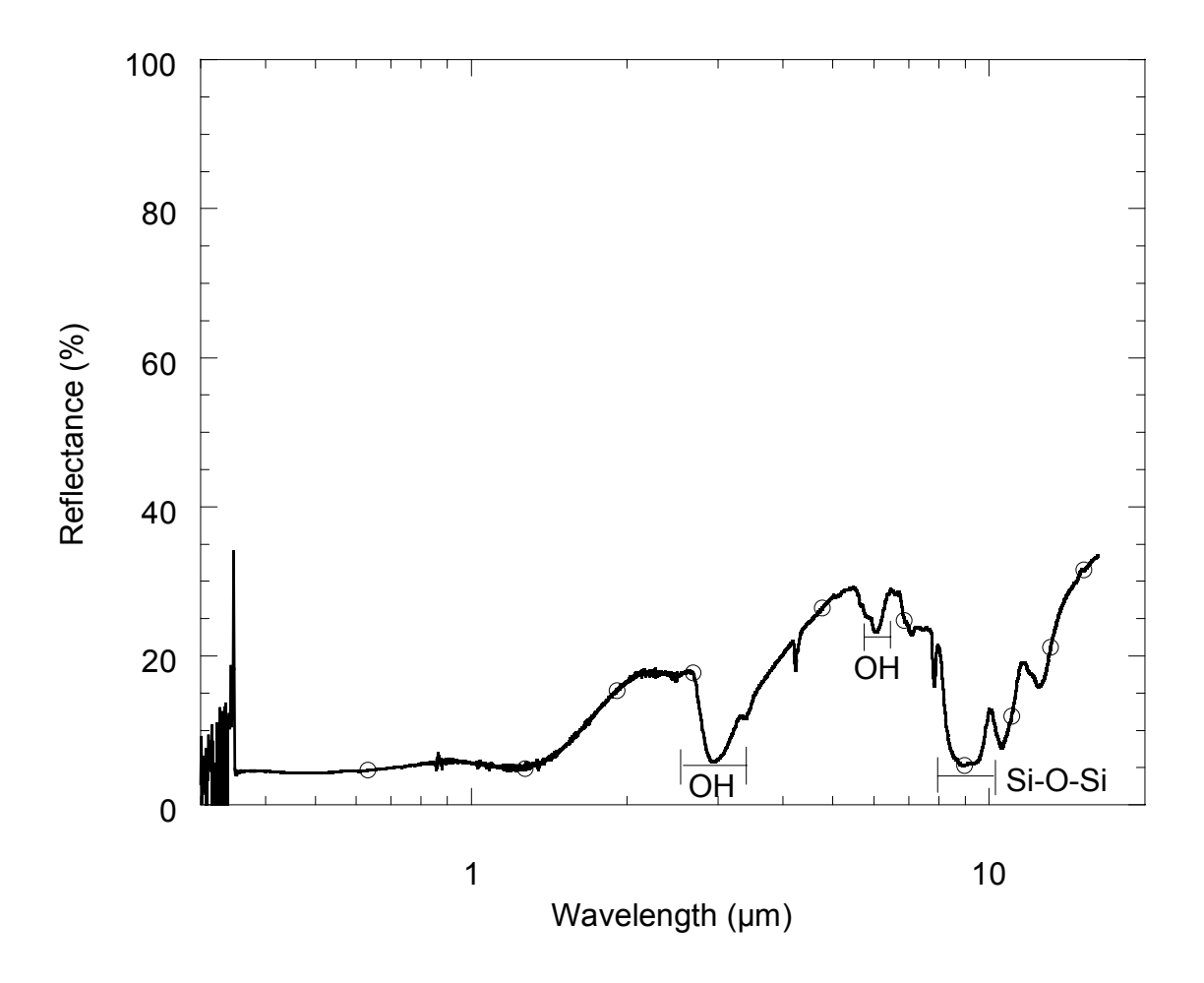


Figure 4.9. Spectral reflectance of a C-SiO $_{2}$ sample

The reflectance of the sample under study was generally very low in all the studied wavelength ranges. An attempt to find out why this was so was done by scanning a sample provided by Katumba (see Katumba *et al.* [7]). The IR reflectance spectra of the sample were obtained using

a fourier transform infrared (FTIR) Bomem-Michelson 110 spectrophotometer and a Buck M500 IR spectrophotometer. The two spectra are shown in Figure 4.10.

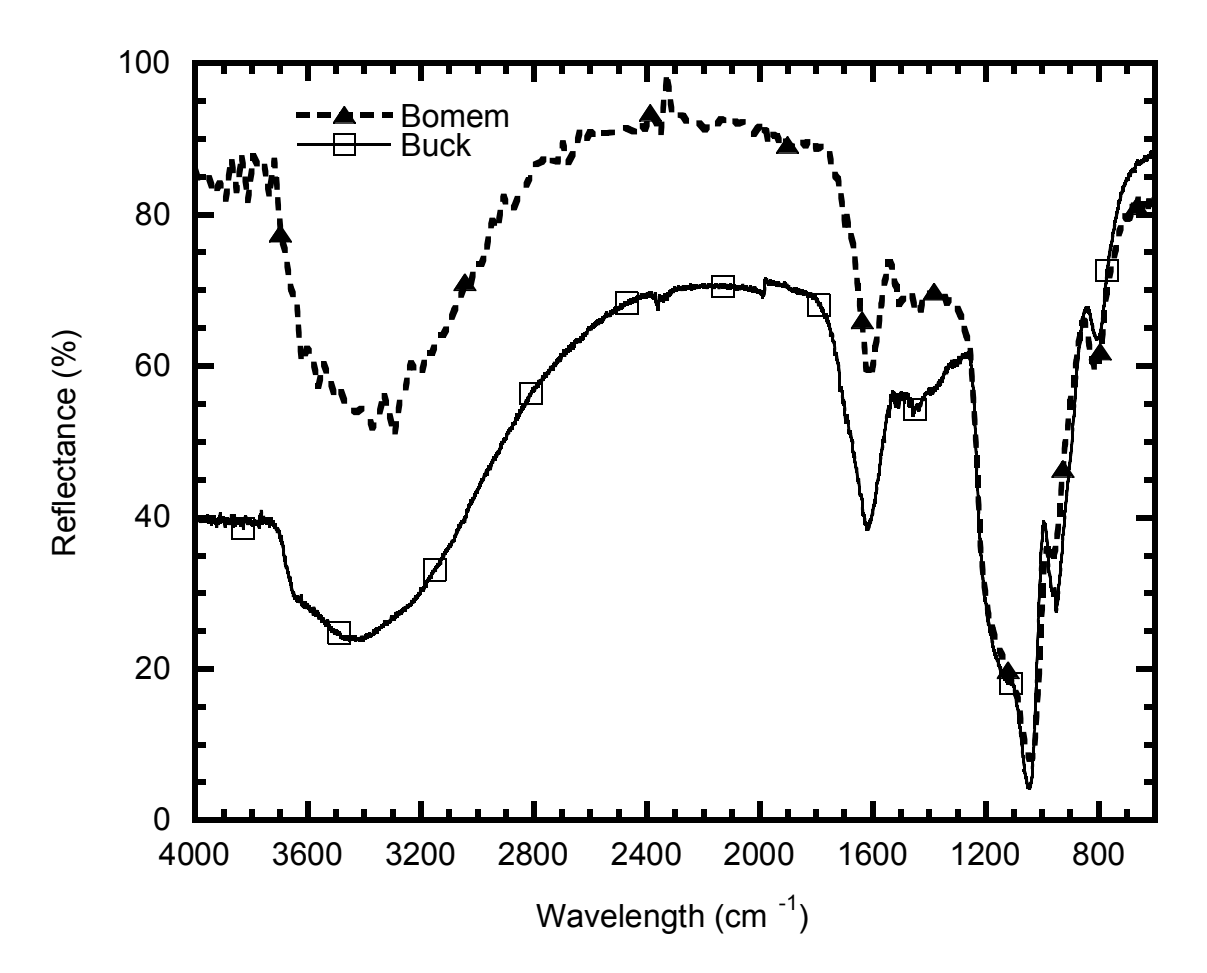


Figure 4.10. Comparison of spectra obtained from two spectrophotometers: FTIR Bomem-Michelson 110 with integrating sphere and Buck M500 IR without.

The FTIR Bomem-Michelson 110 spectrophotometer gave a spectrum showing higher reflectance whilst the spectrum obtained from the Buck M500 IR spectrophotometer had lower reflectance. The reason for this is that the first spectrophotometer had an integrating sphere whilst the later did not have. This means that the Bomem measured both the specular and the diffuse reflectance whilst the Buck measured the specular reflectance only.

4.4.1. Effect of heat-treatment temperature on C-SiO₂/Al samples

Figure 4.11 shows the variation of the reflectance of C-SiO₂/Al samples with heat treatment temperature. In the solar spectral range, the reflectance increases with heat-treatment temperature. Samples heat-treated at 300 °C and 400 °C have the lowest reflectance and samples heat-treated at 550 °C have the highest reflectance. One would expect the reflectance to decrease with heat-treatment temperature since the carbon content is expected to increase.

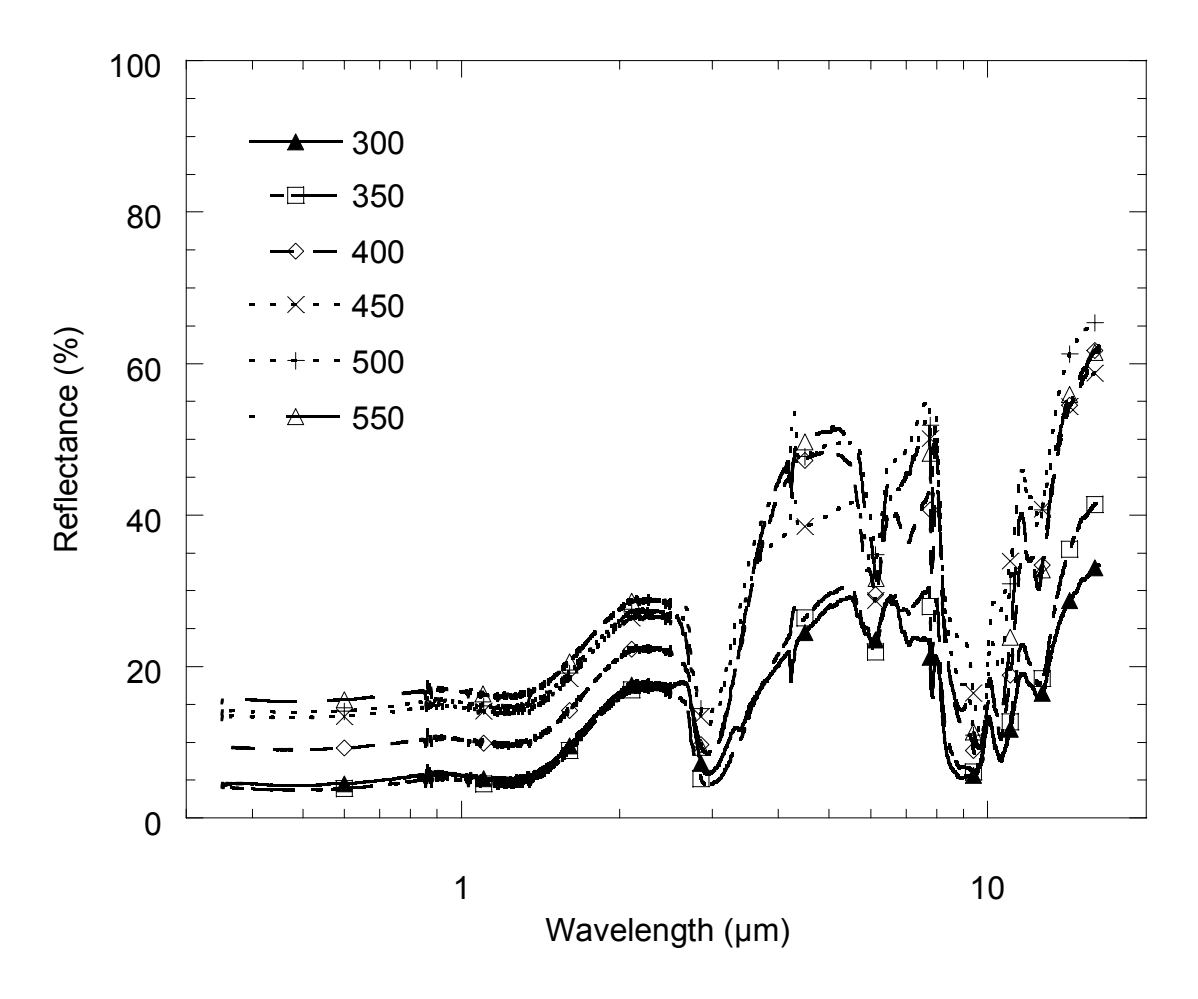


Figure 4.11. Effect of heat-treatment temperature on $\text{C-SiO}_2/\text{Al}$ samples

The transition from low reflectance to high reflectance occurs at about 3 μm . It shifts towards shorter wavelengths as the heat treatment temperature is increased. No noticeable change of order occurs in the IR except that the samples heat-treated at 500 °C now have the highest reflectance. Generally the reflectance is low. This is due to the fact that the instrument only

measures specular reflectance. Another contributing factor is that the samples developed cracks even though MTES was used in the fabrication [7]. The cracks increase the amount of diffuse reflection.

Table 4.6 shows the variation of the α_{sol} / ϵ_{therm} ratio with heat treatment temperature. The ratio increases with temperature up to 500 °C where it has a maximum value. There is a decrease in the ratio at 550 °C.

Table 4.6. The dependence of the ratio of solar absorptance to thermal emittance of C-SiO₂/Al with heat-treatment temperature.

Temperature (°C)	Absorptance, α_{sol}	Thermal emittance,	$\alpha_{sol}/\ \epsilon_{therm}$
		$\epsilon_{ m therm}$	
300	0.9378	0.8288	1.1315
350	0.9442	0.8016	1.1779
400	0.8908	0.6963	1.2793
450	0.8488	0.6621	1.2820
500	0.8417	0.6462	1.3025
550	0.8270	0.6776	1.2205

4.4.2. Effect of heat-treatment temperature on C-SiO₂/steel samples

Figure 4.12 shows the variation of reflectance of C-SiO₂/steel with heat treatment temperature. In the solar spectral range, the reflectance increases with heat-treatment temperature up to 400 °C at which it starts to decrease. Samples heat-treated at 300 °C have the lowest reflectance.

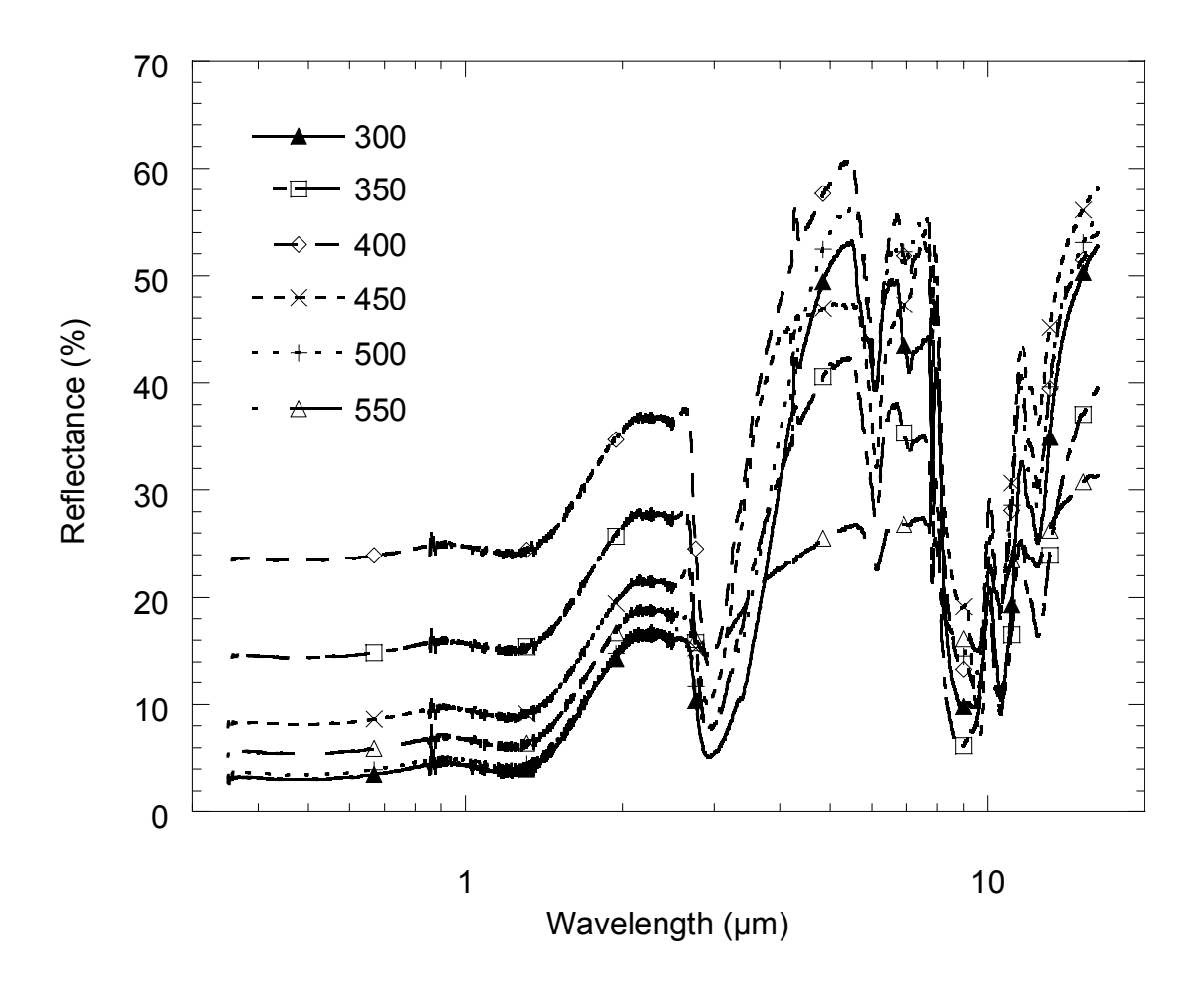


Figure 4.12. The effect of heat-treatment temperature on $C-SiO_2/steel$ samples

One could expect an increase in the absorptance as the heat treatment temperature increases. This is because the samples become darker with increase of heat treatment temperature. Samples heat-treated at temperatures above 400 °C behaved as expected. Their absorptance increases with heat-treatment temperature. This is attributed to the darkening of the steel substrates when heated.

In the IR range, the samples heat-treated at 400 °C have the highest reflectance. The samples heat-treated at 300 °C have a comparatively high reflectance though they have the lowest reflectance in the solar spectral range. Samples heat-treated at 550 °C have the lowest reflectance in this range. This is also attributed to the change in the properties of steel as it is heated.

Table 4.7 shows the variation of α_{sol} / ϵ_{therm} ratio with heat-treatment temperature. The maximum is obtained for samples heat treated at 500 °C.

Table 4.7. The dependence of the ratio of solar absorptance to thermal emittance of C-SiO₂/steel samples with heat-treatment temperature.

Temperature (°C)	Absorptance, α_{sol}	Absorptance, α_{sol} Thermal emittance,	
		$\epsilon_{ m therm}$	
300	0.9507	0.6025	1.5779
350	0.8371	0.7012	1.1938
400	0.7470	0.5577	1.3394
450	0.8997	0.5492	1.6382
500	0.9462	0.5600	1.6896
550	0.9268	0.7382	1.2555

4.5. Limits of absorptance and emittance

The various combinations of solar absorptance and thermal emittance of the C-NiO samples used in this investigation are shown in Figure 4.13. The graph shows that the limit for absorptance is about 0.94 and that for the emittance is 0.12. The optimum figures achieved in a single sample are 0.63 for absorptance and 0.11 for emittance. Comparative figures for C-NiO absorbers have not been found in the available literature. Ni-NiO_x absorbers on aluminium substrates produced by reactive sputtering [3] have an absorptance of 0.96 and an emittance of 0.10.

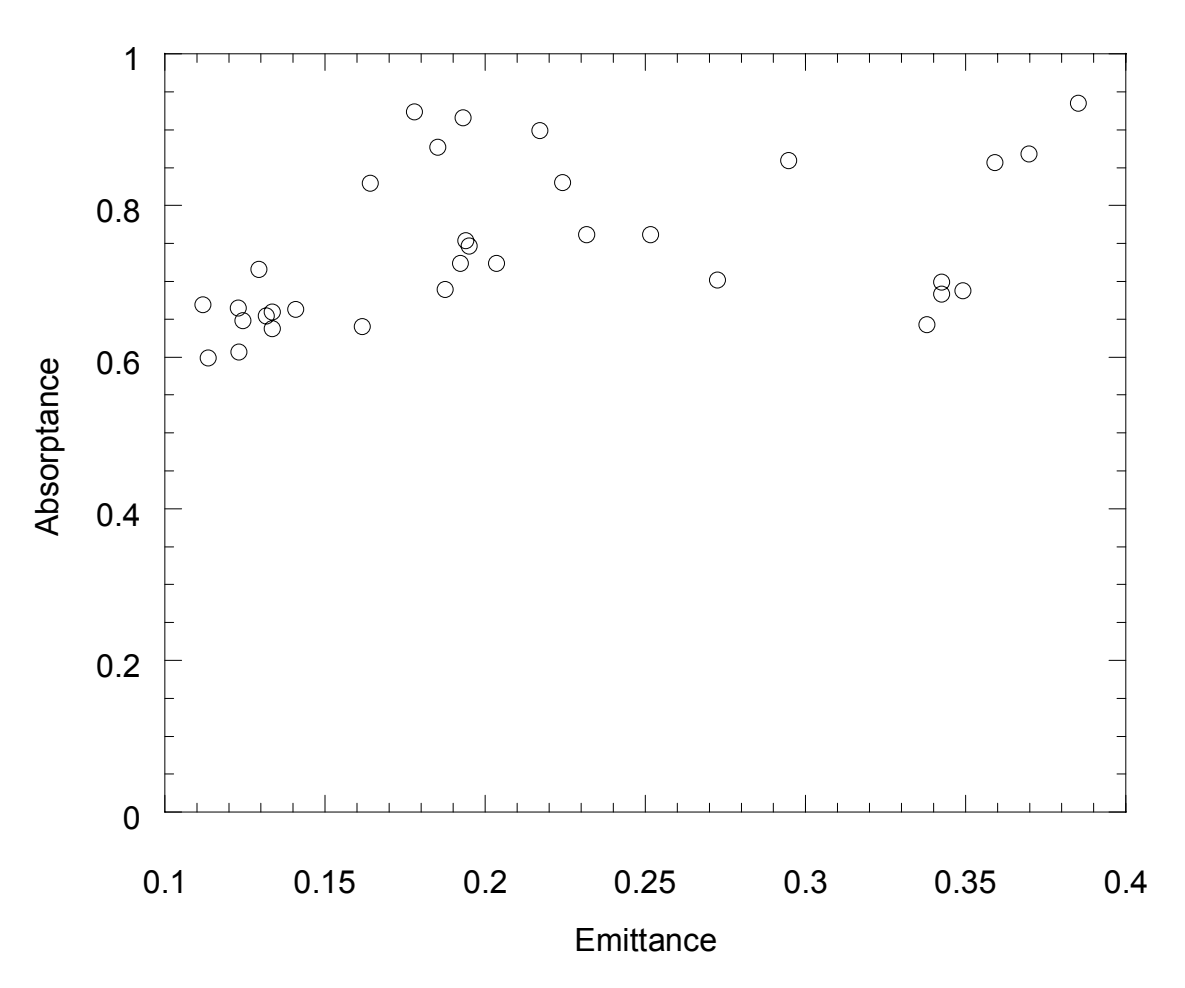


Figure 4.13. Scatter graph of absorptance and emittance of all types of C-NiO samples used in this investigation.

The various combinations of solar absorptance and thermal emittance of the C-SiO₂ samples used in this investigation are shown in Figure 4.14. The graph shows that the limit for absorptance is

about 0.95 and that for the emittance is 0.55. The optimum figures achieved in a single sample are 0.93 and 0.56. The higher emittance values are due to the fact that C-SiO₂ samples had cracks that scatter much of the incident radiation and also that the spectrophotometer used did not have an integrating sphere to measure all the reflected radiation.

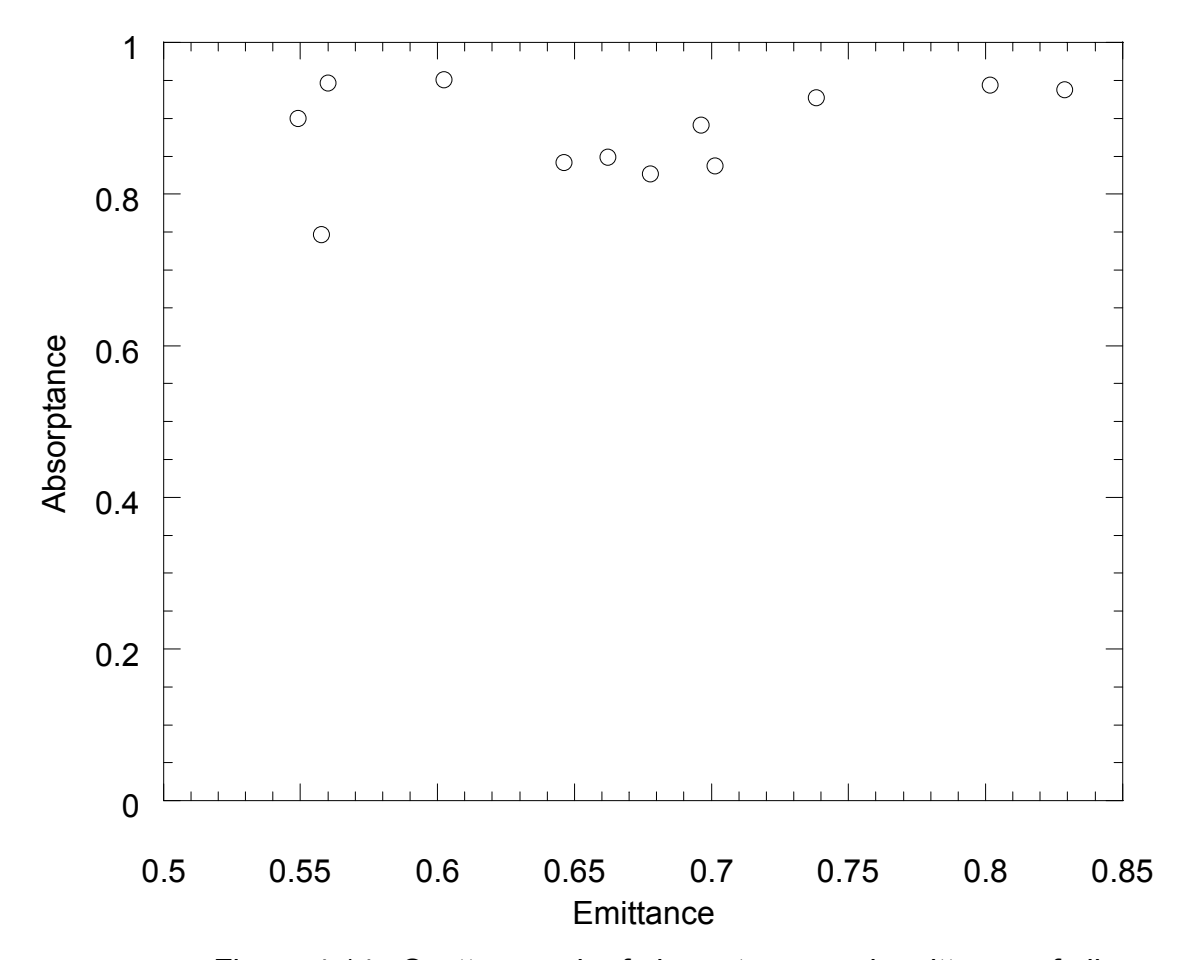


Figure 4.14. Scatter graph of absorptance and emittance of all C-SiO_2 samples used in this investigation.

Comparative figures for similar C-SiO₂ absorbers are 0.88 for absorptance and 0.41 for emittance [7].

CHAPTER 5. CONCLUSIONS AND RECOMMENDATIONS

5.1. Conclusions

This work has demonstrated that it is possible to fabricate low cost selective solar absorbers using readily available materials by the sol-gel process. C-NiO and C-SiO₂ samples were fabricated on Al and steel substrates.

Optical characterization measurements were made in the solar spectral and IR ranges using the available spectrophotometers. All the measurements have been carried out at room temperature.

C-NiO samples were optimized for SUC and PEG content and also for spin coating speed. The experiments showed that increasing SUC content increases the absorptance and lowers the emittance (Figure 4.3). This is in agreement with the observations of Katumba *et al.* [7]. The optimum for samples with high absorptance and low emittance was chosen to be 8 g SUC and was used for the rest of the experiments. Addition of PEG resulted in an increase in both the absorptance and emittance (Figure 4.4). This is not wanted but a realization that PEG increases the porosity of the films makes it useful. The optimum PEG content was chosen as 1.0 g and was used for the rest of the experiments.

The absorptance was found to increase with spin coating speed (Figure 4.5). This is in disagreement with Katumba *et al.* [7]. The suggested reason was linked to the reduction reaction between carbon and NiO. The speed that had the highest $\alpha_{sol}/\epsilon_{therm}$ value was considered to be the optimum and a value of 3000 rpm was identified and used for the rest of the experiments.

An investigation of the effects of heat treatment temperature of C-NiO samples on aluminium (Figure 4.6) and steel substrates (Figure 4.7) showed similar results. The optimum temperature for the samples on all the substrates was obtained as 350 °C. There are differences for temperatures above 400 °C. Samples on aluminium substrates do not show a marked change in absorptance but samples on steel substrates show an increase in absorptance.

A similar research carried out using C-SiO₂ samples on the two substrates mentioned above (Figures 4.11 and 4.12) showed that the optimum temperature occurred at a higher temperature. It was 500 °C for both samples. The cause for this is that the reduction reaction does not occur in C-SiO₂ samples and so the carbonization takes place until it is complete.

A comparison of the two composites shows that the C-NiO absorbers can be manufactured at a lower temperature than C-SiO₂ absorbers. The disadvantage with C-NiO absorbers is that the reduction reaction occurs as the temperature is raised which makes them not applicable for high temperature applications. C-SiO₂ absorbers can be used in a high temperature environment without a problem. The drawback is the cracking, which takes place on the absorbing surface. This scatters the radiation and reduces the absorptance. This has been investigated by comparing two spectra for the same sample obtained using a spectrophotometer with an integrating sphere and one without. The results show that the spectrophotometer without an integrating sphere recorded comparatively lower reflectance values where the other one recorded higher values.

The effect of heating steel substrates was investigated independently (Figure 4.8). It was found out that steel changes optical properties and colour when heated. Its absorptance increases and its emittance also increases with increase in treatment temperature.

5.2. Recommendations and suggestions for further research

The reflectance of all samples in the IR range was measured using a spectrophotometer without an integrating sphere. Carrying out the measurements using an instrument with an integrating sphere could improve the results. The Physics Department of the University of Zimbabwe is recommended to purchase a spectrophotometer that can measure total reflectance.

The need for substrates that are not scratched cannot be over-emphasized. Substrates with scratches contribute to the production of non-uniform films. This contributes much to the scattering of the radiation during optical characterization.

The facilities to analyze the morphology of the films should be made available. Researchers from established laboratories make use of instruments like scanning electron microscopes (SEM) to study the morphology of their films.

I also suggest the use of physical models in the calculation of optical parameters of these composites. This helps in the optimization process.

REFERENCES

- [1] P. Nostell, PhD Thesis, Preparation and Optical Characterization of Antireflection Coatings and Reflector Materials for Solar Systems, University Printers, Uppsala, Sweden (2000).
- [2] T. Tesfamichael, DPhil Thesis, Characterization of Selective Solar Absorbers:

 Experimental and Theoretical Modeling, University Printers, Uppsala, Sweden, 2000.
- [3] C. E. Kennedy, *Technical Report: Review of Mid-to-High-temperature Solar Selective Absorber Materials*, National Renewable Energy Laboratory, prepared under Task No. CP02.2000, NREL/TP-520-31267 (2002).
- [4] K. Gelin, DPhil Thesis, *Preparation and Characterization of Sputter Deposited Spectrally Selective Solar Absorbers*, University Printers, Uppsala, Sweden (2004).
- [5] D. Chen, Y. Yan, E. Westenberg, D. Niebauer, N. Sakatani, S. R. Chaudhuri, Development of Anti-Reflection (AR) Coating on Plastic Panels for Display Applications, Journal of Sol-Gel Science and Technology 19, 77-82 (2000).
- [6] P. Nostell, A. Roos, B. Karlsson, *Antireflection of glazings for solar energy applications*, Solar Energy Materials and Solar Cells **54**, 223-233 (1998).
- [7] G. Katumba, J. Lu, L. Olumekor, G. Westin, E. Wäckelgård, Low Cost Selective Solar Absorber Coatings: Characteristics of Carbon-In-Silica Synthesized with Sol-Gel Technique, Journal of Sol-Gel Science and Technology 36, 33-43 (2005).
- [8] P. S. Haddad, F. F. Ferreira, G. E. S. Brito, M. C. A. Fantini, *Gold–Nickel Hydroxide*Multi Layers with Selective Absorption in the Visible Range, Journal of Sol-Gel Science and Technology **30**, 179-185 (2004).

- [9] J. D. Mackenzie, E. P. Bescher, *Physical Properties of Sol-Gel Coatings*, Journal of Sol-Gel Science **19**, 23-29 (2000).
- [10] G. Katumba, J. Lu, L. Olumekor, G. Westin, E. Wäckelgård, Low Cost Selective Solar Absorber Coatings: Characteristics of Carbon-In-Silica Synthesized with Sol-Gel Technique, Journal of Sol-Gel Science and Technology 36, 36 (2005).
- [11] Z. Liu, Z. JIN, J. Qui, Preparation of porous thin films by sol-gel method using PEG template, Materials Letters **59**, 3620-3625 (2005).
- [12] J. C. Maxwell, *A dynamical theory of the electromagnetic field*, in "The scientific papers of James Clerk Maxwell," Vol. 1 edited by W. D. Niven, Cambridge University Press, London (1890).
- [13] P. Konttinen, *PhD Thesis: Characterization and aging studies of selective solar C/Al₂O₃/Al absorber surfaces*, Helsinki University of Technology, Finland (2004).
- [14] R. Siegel, J. R. Howel, *Thermal Radiation Heat Transfer*, Third Edition, (Hemisphere Publishing Corporation, Washington, 1992), Chapter 1.
- [15] J. A. Duffie, W. A. Beckman, *Solar Engineering of thermal processes*, 2nd Edition, John Wiley and Sons, New York (1991).
- [16] R. V. Dunkle, *Thermal radiation*. *Tables and* Applications, Trans, ASME **76**, 549 (1954).
- [17] S. L. Sargent, A compact table of blackbody radiation functions, Bull of the Am. Meteorological Soc 53, 360 (1972).
- [18] I. M. Thomas, in Sol-Gel Optics: Processing and Applications, *Optical coating fabrication*, Edited by L. C. Klein, Kluwer Academic Publishers, Bolston, 1994 page 141.
- [19] C. J. Brinker and G. W. Scherer, *Sol-Gel Science The Physics and Chemistry of Sol-Gel Processing*, (Academic Press, San Diego, 1990) chapter 1.

- [20] C. J. Brinker and G. W. Scherer, *Sol-Gel Science The Physics and Chemistry of Sol-Gel Processing*, (Academic Press, San Diego, 1990) chapter 13.
- [21] E. M. Rabinovick, in Sol-Gel optics: Processing and Applications, *Sol-Gel Processing-General Principles*, edited by L. C. Klein, Kluwer Academic Publishers, Bolston, 1994.
- [22] C. J. Brinker and G. W. Scherer, *Sol-Gel Science The Physics and Chemistry of Sol-Gel Processing*, (Academic Press, San Diego, 1990) chapter 14.
- [23] C. J. Brinker and G. W. Scherer, *Sol-Gel Science The Physics and Chemistry of Sol-Gel Processing*, (Academic Press, San Diego, 1990) chapter 8.
- [24] J. Livage, F. Babonneau, C. Sanhez, in Sol-Gel Optics: Processing and Applications, *Solgel chemistry for optical materials*, Edited by L. C. Klein, Kluwer Academic Publishers, Bolston, 1994 page 38.
- [25] L. Zhifeng, J. Zhengguo, L. Wei, Q. Jijun, *Preparation of ZnO porous thin films by sol-gel method using PEG template*, Materials Letters **59**, 3620-3625 (2005).
- [26] P. Nostell, A. Roos, B. Karlsson, *Optical and mechanical properties of sol-gel antireflective films for solar energy applications*, Thin Solid Films **351**, 170-175 (1999).
- [27] A. Pohl, Sol-Gel Synthesis of CMR Manganites, Acta Universitatis Upsaliensis, Uppsala (2004)
- [28] J. Hernández-Torres, A. Mendoza-Galván, Formation of NiO-SiO₂ nanocomposite thin films by the sol-gel method, Journal of Non-crystalline Solids **351**, 2029-2035 (2005).
- [29] Q. Yang, J. Sha, X. Ma, D. Yang, Synthesis of NiO nanowires by the sol-gel process, Materials Letters **59**, 1967-1970 (2005).
- [30] R. M. Almeida, *Spectroscopy and Structure of Sol-Gel Systems*, Journal of Sol-Gel Science and Technology **13**, 51-59 (1998).

- [31] A. E. Jiménez-González, J. A. Soto Urueta, R. Suárez-Parra, Optical and electrical characterization of aluminium-doped ZnO thin films prepared by sol-gel technique, Journal of Crystal Growth 192, 430-438 (1998).
- [32] P. S. Haddad, F. F. Fereira, G.E.S. Brito, M. C. A. Fantini, *Gold-Nickel hydroxide multi-layers with selective absorption in the visible range*, Journal of Sol-gel Science and Technology **30**,179-185 (2004).
- [33] P. Konttinen, R. Kulpi, P. D. Lundi, *Microstructural analysis of selective C/Al₂O₃/Al solar absorber surfaces*, Thin Solid Films **425**, 24-30 (2003).
- [34] P. Konttinen, P. D. Lundi, *Characterization of selective absorbers prepared through a mechanical treatment*, Invited Lecture, in Proceedings of the World Renewable Energy Congree VII. Cologne, Germany, 29 June 5 July 2002.
- [35] P. Konttinen, P. D. Lundi, *Mechanically manufactured selective solar absorber surfaces*, Solar Energy Materials and Solar Cells **79**, 273-283 (2003).
- [36] P. Konttinen, P. D. Lundi, *Thermal stability and moisture resistance of C/Al₂O₃/Al solar absorber surfaces*, Solar Energy Materials and Solar Cells **82**, 361-373 (2004).
- [37] P. Konttinen, P. D. Lundi, *Microstructural optimization and extended studies of low cost rough graphite-aluminium solar absorber surfaces*, Renewable Energy **29**, 823-839 (2004).
- [38] P. Konttinen, P. D. Lundi, *Physical interpretation of impacts from a low cost manufacturing process on the surface microstructure of a novel solar absorber*, Solar Energy Materials and Solar Cells **84**, 171-181 (2004).
- [39] P. Konttinen, T. Salo, P. D. Lund, Degradation of unglazed rough graphite-aluminium solar absorber surfaces in simulated acid and neutral rain, Solar Energy 78, 41-48 (2005).

- [40] G. Makiwa, *Industrial Attachment in the Physics Department of the University of Zimbabwe*, University of Zimbabwe (2005).
- [41] Science Data Book, Edited by R. M. Tennent, Longman House, Oliver and Boyd (1993) page 51.
- [42] European Standard, Thermal insulation of glazing-Calculation rules for determining the steady "U" value (thermal transmittance) of glazing, EN673 (1998).
- [43] G.A. Niklasson, C. G. Granqvist, *Selectively solar-absorbing surface coatings: Optical properties and degradation*, edited by C. G. Granqvist in Material Science for Solar Energy Conversion Systems, Renewable Energy Series, Pergamon Press, Oxford (1991) Chapter 4.
- [44] G. Pellegrini, Experimental methods for the preparation of selectively absorbing textured surfaces for photo-thermal solar conversion, Solar Energy Materials 3, 391 (1980).
- [45] E. Randrich, D. D. Allred, *Chemical vapour-deposited ZrB*₂ as a selective solar absorber, Thin Solid Films **83**, 393 (1981).
- [46] B. O. Seraphin, Chemical vapour deposition of thin films for solar energy conversion, Thin Solid Films **39**, 87 (1976).
- [47] J. W. Twidell, A. D. Weir, *Renewable energy resources*, The University Press, Cambridge, London (1986), pg 104.
- [48] R. Siegel, J. R. Howel, *Thermal Radiation Heat Transfer*, Third Edition, (Hemisphere Publishing Corporation, Washington, 1992), Chapter 4.
- [49] S. Svanberg, *Atomic and molecular spectroscopy-Basic aspects and practical applications*, 2nd Edition, Springer (1992).
- [50] Z. Chiguvare, MSc Thesis, *Design and construction of a reflectance spectrometer for the analysis of spectral surface phenomena*, University of Zimbabwe (1997).

- [51] D. A. G. Bruggman, Annalender Physics 24, 636 (1935).
- [52] Q. C. Zhang, *Optimizing analysis of W-AlN cermet solar absorbing coatings*, J. Phys. D: Appl. Phys **34**, 3114-3120 (2001).
- [53] J. C. Maxwell Garnett, Philos. Trans. R. Soc (London) 203, 385 (1904); 205, 237 (1906).
- [54] H. Tabor, Trans., Conference on the use of solar energy, 2, 1A, Tucson, Arizona (1956).

APPENDICES

APPENDIX A: List of symbols and abbreviations

Symbol	Definition
$lpha_{sol}$	solar absorptance
A_c	collector area
C_I	Plank's first radiation constant (m ² W)
C_2	Plank's second radiation constant (mK)
arepsilon	complex dielectric function
$arepsilon_{I}$	real part of dielectric function
$arepsilon_2$	complex part of dielectric function
$arepsilon_{BR}$	effective dielectric function from the Bruggeman model
$arepsilon_{MG}$	effective dielectric function from the Maxwell Garnett model
\mathcal{E}_{therm}	thermal emittance
G_T	total solar energy flux
κ	extinction coefficient
I	total irradiance onto the collector plane (Wm ⁻¹)
I_B	total hemispherical energy emited by a blackbody (Jm ⁻¹)
λ	wavelengths
n	refractive index
$n_{e\!f\!f}$	effective refractive index
η	efficiency
Q_u	collector array thermal output (Wm ⁻¹)
R	ideal gas constant = $8.3143 \text{ (Jmol}^{-1}\text{K}^{-1}\text{)}$
θ	incidence angle of light

T temperature

 T_a ambient temperature

 T_p absorber plate temperature

μm microns

 U_L heat transfer coefficient

Abbreviations

AFM atomic force microscopy

AM air-mass

AR Antireflective

CVD Chemical-vapour deposition

DEA Diethanolamine

FTIR Fourier transform infrared

IR Infrared

ISO International Organisation for Standards

MTES methyl trimethoxysilane

NIR near infrared

PEG Polyethylene glycol

pH hydrogen ion concentration

PV photo-voltaic

PVD physical vapour deposition

SEM scanning electron microscopy

SS stainless steel

SUC sucrose

TEOS tetraethyl orthosilicate

UV Ultraviolet

Vis Visible

XRD X-ray diffraction

APPENDIX B: Definitions

Definitions

Air Mass: The ratio of the optical thickness of the atmosphere through which beam

radiation passes to the optical thickness if the sun were at the zenith.

Cermet: A metal-dielectric composite.

Colloid: A suspension in which the dispersed phase is so small (~1-1000 nm) that

gravitational forces are negligible and interactions are dominated by short-

range forces, such as van der Waals attraction and surface charges.

Diffuse radiation: The solar radiation received from the sun after its direction has been

changed by scattering by the atmosphere.

Direct solar radiation: The solar radiation received from the sun without having been scattered by

the atmosphere.

Emulsion: A suspension of liquid droplets in another liquid.

Gel: A two-component system of a semi-solid nature, rich in liquid.

Irradiance: The rate at which radiant energy is incident on a surface, per unit area of

surface

Microstructure: The microscopic structure of a material.

Morphology: The external form and structure of a material or topographic features.

Sol: A colloidal suspension of solid particles in a liquid.

Sol-gel: A wet chemical route for the synthesis of colloidal dispersions of inorganic

and organic-inorganic hybrid materials, particularly oxides and oxide-

based hybrids.

Total solar radiation: The sum of the beam and the diffuse radiation a surface.

Zenith: The point directly overhead

APPENDIX C: Blackbody radiation data

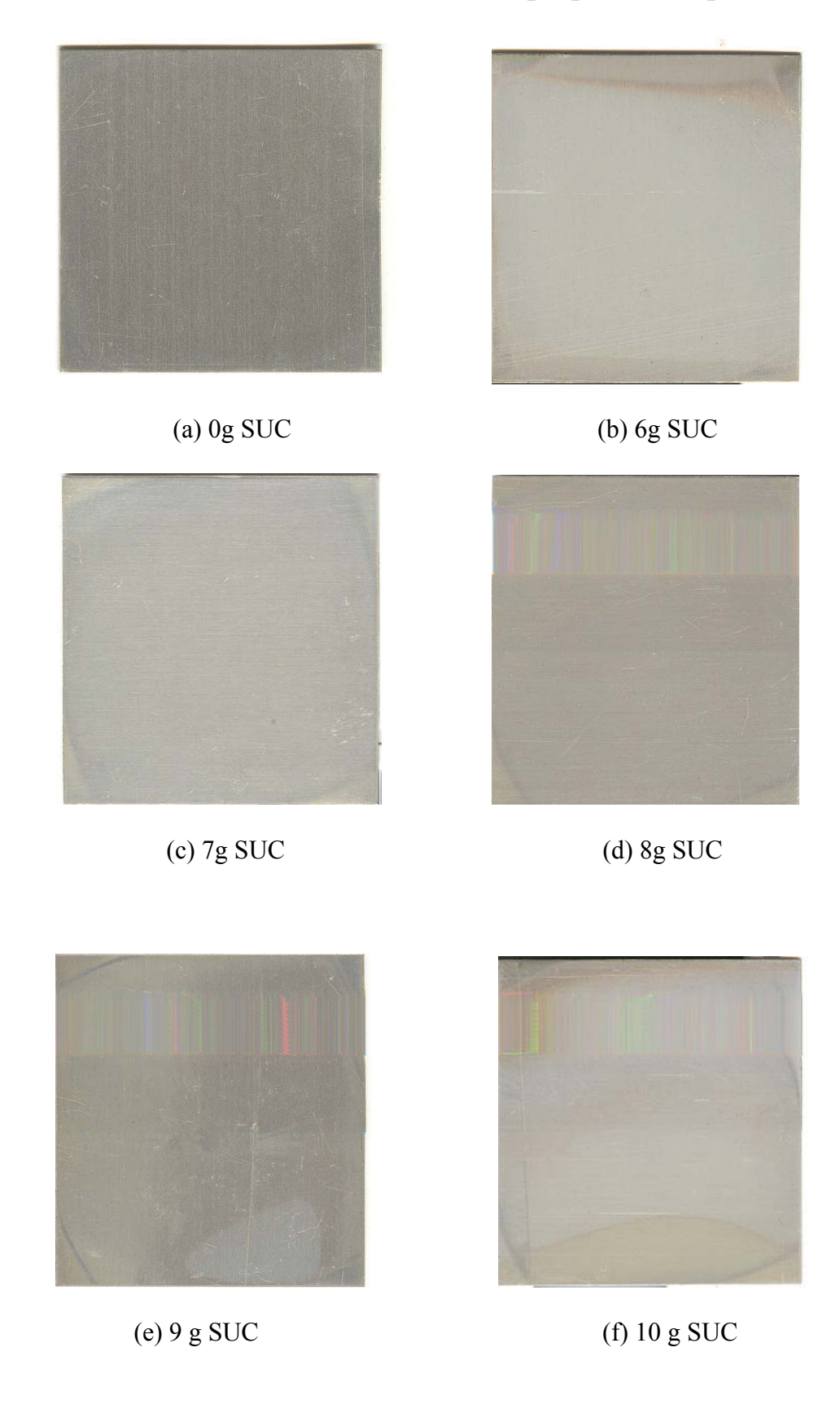
Table C1. Fraction of blackbody radiation energy between zero and λT for even increments of λT .

λT , μ mK	$f_{o-\lambda T}$	λT , μ mK	$f_{o-\lambda T}$	λT , μ mK	$f_{o-\lambda T}$
1000	0.0003	4500	0.5643	8000	0.8562
1100	0.0009	4600	0.5793	8100	0.8601
1200	0.0021	4700	0.5937	8200	0.8639
1300	0.0043	4800	0.6075	8300	0.8676
1400	0.0077	4900	0.6209	8400	0.8711
1500	0.0128	5000	0.6337	8500	0.8745
1600	0.0197	5100	0.6461	8600	0.8778
1700	0.0285	5200	0.6579	8700	0.8810
1800	0.0393	5300	0.6693	8800	0.8841
1900	0.0521	5400	0.6803	8900	0.8871
2000	0.0667	5500	0.6909	9000	0.8899
2100	0.0830	5600	0.7010	9100	0.8927
2200	0.1009	5700	0.7107	9200	0.8954
2300	0.1200	5800	0.7201	9300	0.8980
2400	0.1402	5900	0.7291	9400	0.9005
2500	0.1613	6000	0.7378	9500	0.9030
2600	0.1831	6100	0.7461	9600	0.9054
2700	0.2053	6200	0.7541	9700	0.9076
2800	0.2279	6300	0.7618	9800	0.9099
2900	0.2506	6400	0.7692	9900	0.9120
3000	0.2732	6500	0.7763	10000	0.9141
3100	0.2958	6600	0.7831	11000	0.9318
3200	0.3181	6700	0.7897	12000	0.9450
3300	0.3401	6800	0.7961	13000	0.9550
3400	0.3617	6900	0.8022	14000	0.9628
3500	0.3829	7000	0.8080	15000	0.9689
3600	0.4036	7100	0.8137	16000	0.9731
3700	0.4238	7200	0.8191	17000	0.9776
3800	0.4434	7300	0.8244	18000	0.9807
3900	0.4624	7400	0.8295	19000	0.9833
4000	0.4809	7500	0.8343	20000	0.9855
4100	0.4987	7600	0.8390	30000	0.9952
4200	0.5160	7700	0.8400	40000	0.9978
4300	0.5327	7800	0.8479	50000	0.9988
4400	0.5486	7900	0.8521	∞	1

Table C2. Fraction of blackbody radiation energy between zero and λT for even increments of λT .

$f_{o-\lambda T}$	λT , μ mK	λT at	$f_{o-\lambda T}$	λT , μ mK	λT at
		midpoint			midpoint
0.05	1880	1660	0.55	4410	4250
0.10	2200	2050	0.60	4740	4570
0.15	2450	2320	0.65	5130	4930
0.20	2680	2560	0.70	5590	5350
0.25	2900	2790	0.75	6150	5850
0.30	3120	3010	0.80	6860	6480
0.35	3350	3230	0.85	7850	7410
0.40	3580	3460	0.90	9380	8510
0.45	3830	3710	0.95	12500	10600
0.50	4110	3970	1.00	∞	16300

APPENDIX D. The structure of some of the prepared samples.



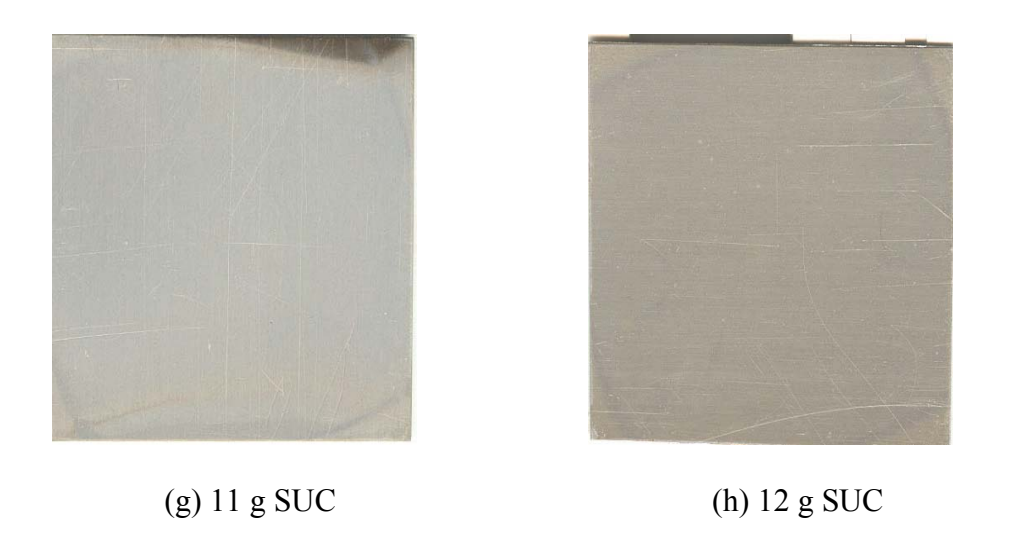
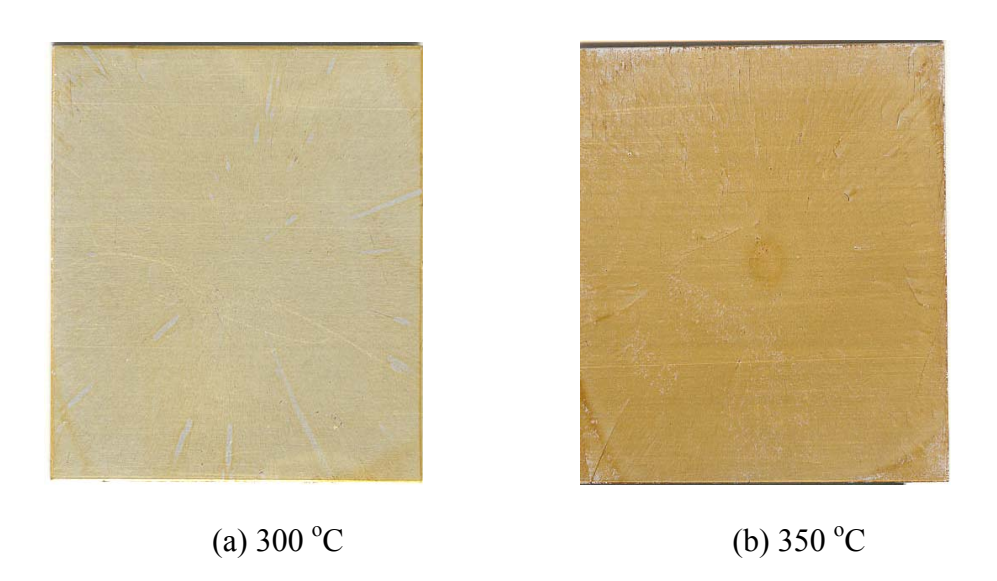


Figure D1. The structure of NiO samples as the SUC content was varied: (a) 0 g SUC, (b) 6 g SUC, (c) 7 g SUC, (d) 8 g SUC, (e) 9 g SUC, (f) 10 g SUC, (g) 11 g SUC and (h) 12 g SUC.



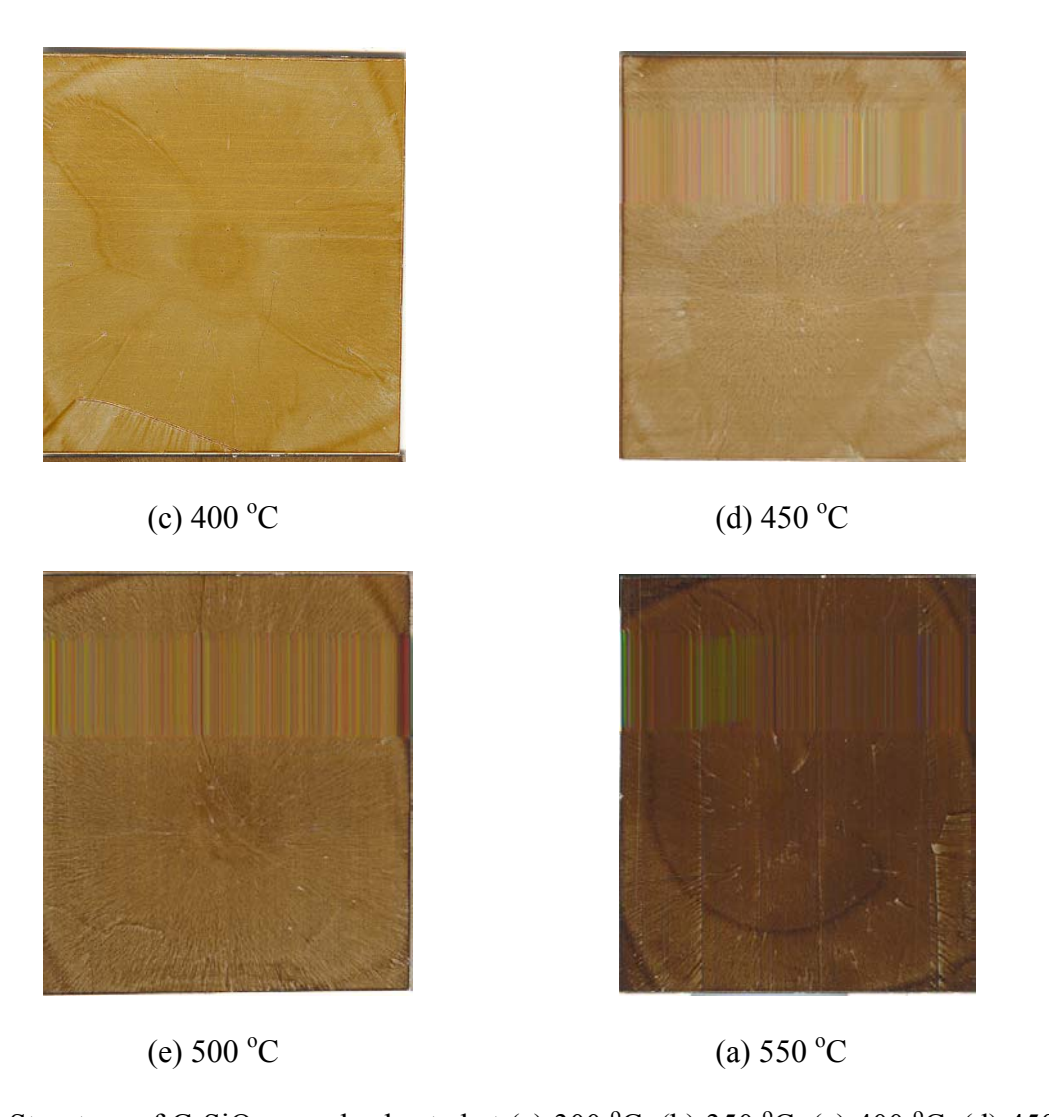
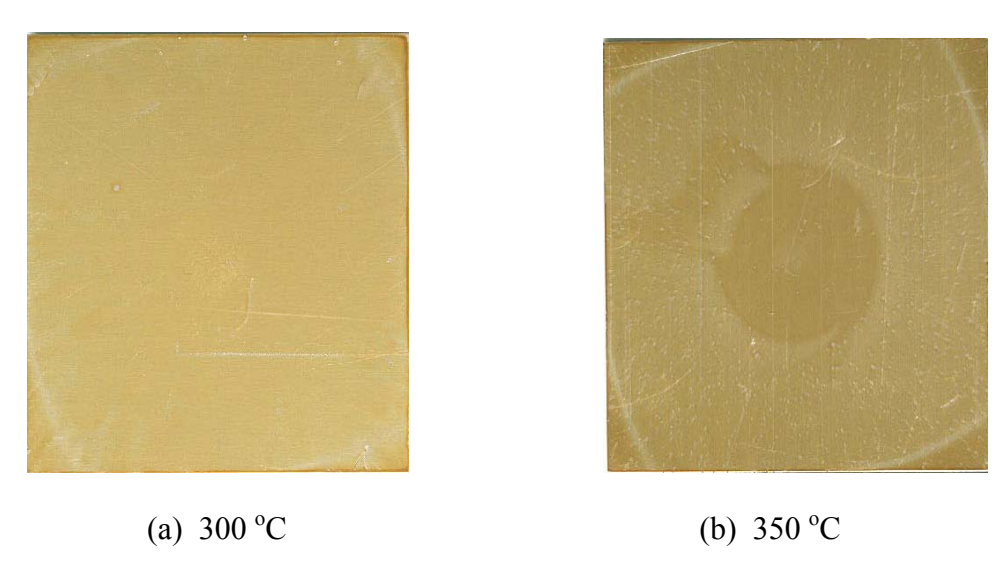


Figure D2. Structure of C-SiO₂ samples heated at (a) 300 $^{\circ}$ C, (b) 350 $^{\circ}$ C, (c) 400 $^{\circ}$ C, (d) 450 $^{\circ}$ C, (e) 500 $^{\circ}$ C and (f) 550 $^{\circ}$ C.



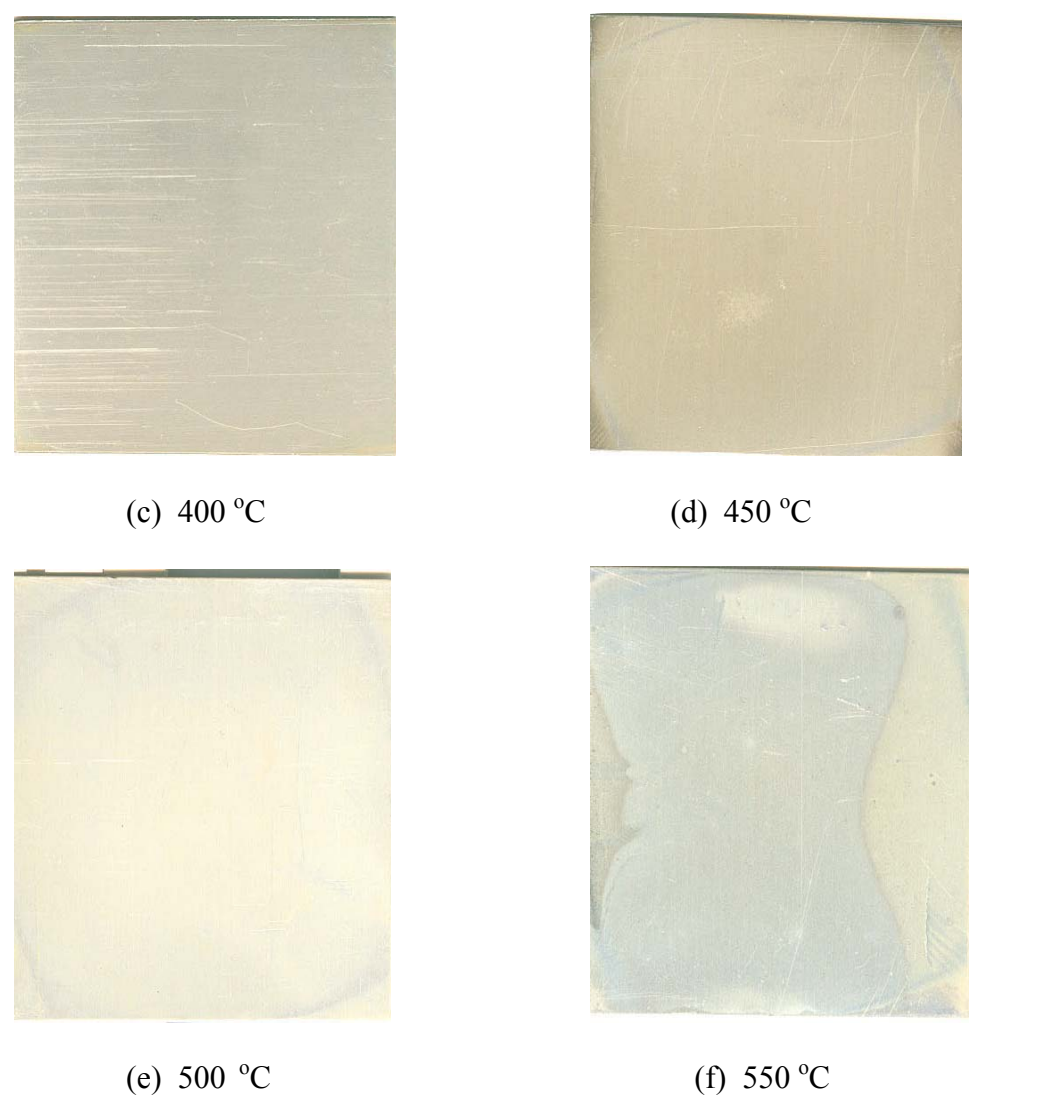


Figure D3. Structure of C-NiO samples heated at (a) 300 $^{\circ}$ C, (b) 350 $^{\circ}$ C, (c) 400 $^{\circ}$ C, (d) 450 $^{\circ}$ C, (e) 500 $^{\circ}$ C and (f) 550 $^{\circ}$ C.